

## The Impact of Universal Extra Dimensions on

$$B \rightarrow X_s \gamma, B \rightarrow X_s \text{ gluon}, B \rightarrow X_s \mu^+ \mu^-,$$

$$K_L \rightarrow \pi^0 e^+ e^- \text{ and } \varepsilon'/\varepsilon$$

Andrzej J. Buras<sup>a</sup>, Anton Poschenrieder<sup>a</sup>  
Michael Spranger<sup>a,b</sup> and Andreas Weiler<sup>a</sup>

<sup>a</sup> Physik Department, Technische Universität München  
D-85748 Garching, Germany

<sup>b</sup> Max-Planck-Institut für Physik - Werner-Heisenberg-Institut  
D-80805 München, Germany

### Abstract

We calculate the contributions of the Kaluza-Klein (KK) modes to the  $\gamma$ -penguins, gluon-penguins,  $\gamma$ -magnetic penguins and chromomagnetic penguins in the Appelquist, Cheng and Dobrescu (ACD) model with one universal extra dimension. Together with our previous calculation of  $Z^0$  penguin diagrams [1] this allows to study the impact of the KK modes on the decays  $B \rightarrow X_s \gamma$ ,  $B \rightarrow X_s \text{ gluon}$ ,  $B \rightarrow X_s \mu^+ \mu^-$  and  $K_L \rightarrow \pi^0 e^+ e^-$  and on the CP-violating ratio  $\varepsilon'/\varepsilon$ . For the compactification scale  $1/R = 300 \text{ GeV}$  the perturbative part of the branching ratio for  $B \rightarrow X_s \mu^+ \mu^-$  is enhanced by 12% while the zero in the  $A_{\text{FB}}$  asymmetry is shifted from  $\hat{s}_0 = 0.162$  to  $\hat{s}_0 = 0.142$ . The sizable suppressions of  $Br(B \rightarrow X_s \gamma)$  (20%) and  $Br(B \rightarrow X_s \text{ gluon})$  (40%) could have interesting phenomenological implications on the lower bound on  $1/R$  provided the experimental and theoretical uncertainties will be decreased. Similar comments apply to  $\varepsilon'/\varepsilon$  that is suppressed relative to the Standard Model expectations with the size of the suppression depending sensitively on the hadronic matrix elements. The impact on  $K_L \rightarrow \pi^0 e^+ e^-$  is below 10%. We point out a correlation between the zero  $\hat{s}_0$  in the  $A_{\text{FB}}$  asymmetry and  $Br(B \rightarrow X_s \gamma)$  that should be valid in most models with minimal flavour violation.

# 1 Introduction

In a recent paper [1] we have calculated the contributions of the Kaluza-Klein (KK) modes to the  $K_L - K_S$  mass difference  $\Delta M_K$ , the parameter  $\varepsilon_K$ , the  $B_{d,s}^0 - \bar{B}_{d,s}^0$  mixing mass differences  $\Delta M_{d,s}$  and rare decays  $K^+ \rightarrow \pi^+ \nu \bar{\nu}$ ,  $K_L \rightarrow \pi^0 \nu \bar{\nu}$ ,  $K_L \rightarrow \mu^+ \mu^-$ ,  $B \rightarrow X_{s,d} \nu \bar{\nu}$  and  $B_{s,d} \rightarrow \mu^+ \mu^-$  in the Appelquist, Cheng and Dobrescu (ACD) model [2] with one universal extra dimension. In this model the only additional free parameter relative to the Standard Model (SM) is the compactification scale  $1/R$ . Thus all the masses of the KK particles and their interactions among themselves and with the SM particles are described in terms of  $1/R$  and the parameters of the SM. This economy in new parameters should be contrasted with supersymmetric theories and models with an extended Higgs sector.

A very important property of the ACD model is the conservation of KK parity that implies the absence of tree level KK contributions to low energy processes taking place at scales  $\mu \ll 1/R$ . In this context the flavour changing neutral current (FCNC) processes considered in [1] are of particular interest as they appear in the SM first at one-loop and are strongly suppressed. Consequently the one-loop contributions from the KK modes to them could in principle be important. Indeed our analysis in [1] has shown that for  $1/R \leq 400$  GeV the KK effects in some of the processes in question could be significant. This is in particular the case of the decays governed by the CKM element  $|V_{ts}|$ , like  $B \rightarrow X_s \nu \bar{\nu}$  and  $B_s \rightarrow \mu^+ \mu^-$ , in which the enhancement through the KK modes in  $Z^0$  penguin diagrams is not softened by the suppression of the relevant CKM parameters in contrast to the processes governed by  $|V_{td}|$ .

In the present paper we extend the analysis of [1] by calculating the decays that receive contributions from the  $\gamma$  penguins, gluon penguins,  $\gamma$ -magnetic penguins and chromomagnetic penguins. In particular we analyze in detail the impact of the KK contributions on the decays  $B \rightarrow X_s \gamma$ ,  $B \rightarrow X_s$  gluon,  $B \rightarrow X_s \mu^+ \mu^-$  and  $K_L \rightarrow \pi^0 e^+ e^-$  and on the CP-violating ratio  $\varepsilon'/\varepsilon$ . Among these processes only the decay  $B \rightarrow X_s \gamma$  has been so far considered in the ACD model in the literature [3]. As we will see our result is consistent with the one obtained by these authors but differs in details.

Of particular interest are the decays  $B \rightarrow X_s \gamma$  and  $B \rightarrow X_s \mu^+ \mu^-$  as the hadronic uncertainties in these decays are moderate and the experimental branching ratios are found to be in the ballpark of the SM expectations. Thus in principle some constraints on the compactification scale  $1/R$  could be obtained from these decays. On the other hand the upper bound on  $K_L \rightarrow \pi^0 e^+ e^-$  is still two orders of magnitude above the predictions of the SM and the decay  $B \rightarrow X_s$  gluon and the ratio  $\varepsilon'/\varepsilon$  are subject to very large hadronic uncertainties. Still, as we will see below, our results for  $B \rightarrow X_s$  gluon and  $\varepsilon'/\varepsilon$  could turn out to be important in the future.

The effects of the KK modes on other processes of interest have been investigated in a number of papers. In [2, 4] their impact on the precision electroweak observables assuming a light Higgs ( $m_H \leq 250$  GeV) and a heavy Higgs led to the lower bound  $1/R \geq 300$  GeV and  $1/R \geq 250$  GeV, respectively. Vacuum stability in a simplified ACD model has been examined in [5].

Subsequent analyses of the anomalous magnetic moment [6], and of the  $Z \rightarrow b\bar{b}$  vertex [7] have shown the consistency of the ACD model with the data for  $1/R \geq 300$  GeV. The latter calculation has been confirmed by us [1].

The scale of  $1/R$  as low as 300 GeV would lead to an exciting phenomenology in the next generation of colliders [8, 9, 10, 11, 12]. Moreover the cosmic relic density of the lightest KK particle as a dark matter candidate turned out to be of the right order of magnitude [13]. The related experimental signatures have been investigated in [14]. In the present paper, as in [1], in order to be more general we will include the results for  $1/R = 200$  GeV that is only slightly below the lowest value of  $1/R = 250$  GeV allowed by electroweak precision data.

As our analysis of [1] shows, the ACD model with one extra dimension has a number of interesting properties from the point of view of FCNC processes discussed here. These are:

- GIM mechanism [15] that improves significantly the convergence of the sum over the KK modes corresponding to the top quark, removing simultaneously to an excellent accuracy the contributions of the KK modes corresponding to lighter quarks and leptons. This feature removes the sensitivity of the calculated branching ratios to the scale  $M_s \gg 1/R$  at which the higher dimensional theory becomes non-perturbative and at which the towers of the KK particles must be cut off in an appropriate way. This should be contrasted with models with fermions localized on the brane, in which the KK parity is not conserved and the sum over the KK modes diverges. In these models the results are sensitive to  $M_s$  and the KK effects in  $\Delta M_{s,d}$  are significantly larger [16] than found in [1]. We expect similar behaviour in the processes considered here.
- The low energy effective Hamiltonians are governed by local operators already present in the SM. As flavour violation and CP violation in this model is entirely governed by the CKM matrix, the ACD model belongs to the class of the so-called models with minimal flavour violation (MFV) as defined in [17]. This has automatically the following important consequence for the FCNC processes considered in [1] and in the present paper: the impact of the KK modes on the processes in question amounts only to the modification of the Inami-Lim one-loop functions [18].
- Thus in the case of the processes considered in [1] these modifications have to be made

in the function  $S$  [19] in the case of  $\Delta M_{d,s}$  and of the parameter  $\varepsilon_K$  and in the functions  $X$  and  $Y$  [20] in the case of the rare decays analyzed there. In order to study the decays  $B \rightarrow X_s \gamma$ ,  $B \rightarrow X_s$  gluon,  $B \rightarrow X_s \mu^+ \mu^-$  and  $K_L \rightarrow \pi^0 e^+ e^-$  and the CP-violating ratio  $\varepsilon'/\varepsilon$  the KK contributions to new short distance functions have to be computed. These are the functions  $D$  (the  $\gamma$  penguins),  $E$  (gluon penguins),  $D'$  ( $\gamma$ -magnetic penguins) and  $E'$  (chromomagnetic penguins). In the ACD model these functions depend only on  $m_t$  and the single new parameter, the compactification radius  $R$ .

Our paper is organized as follows. In section 2, we summarize those ingredients of the ACD model that are relevant for our analysis. In particular, we give in appendix B the set of the relevant Feynman rules involving photons and gluons that have not been given so far in the literature. Further details can be found in [1, 2]. In section 3, we calculate the KK contributions to the penguin functions  $D$ ,  $E$ ,  $D'$  and  $E'$ . In section 4, we analyze the decay  $B \rightarrow X_s \gamma$  and compare our result with the one of [3]. In section 5, we discuss the decay  $B \rightarrow X_s$  gluon. The corresponding analyses of  $B \rightarrow X_s \mu^+ \mu^-$ ,  $K_L \rightarrow \pi^0 e^+ e^-$  and  $\varepsilon'/\varepsilon$  are presented in sections 6, 7 and 8, respectively. In section 9, we summarize our results and give a brief outlook. As a byproduct of our work we point out a correlation between the zero  $\hat{s}_0$  in the  $A_{\text{FB}}$  asymmetry in  $B \rightarrow X_s \mu^+ \mu^-$  and  $Br(B \rightarrow X_s \gamma)$  that should be valid in most models with minimal flavour violation. We also generalize the background field method to five dimensions.

## 2 The Five Dimensional ACD Model

The five dimensional ACD model [2] has been described already in detail in our previous paper [1] where we have given all Feynman rules necessary for the calculations considered there. There are two new features in this work. The first one is the addition of QCD in 5 dimensions which is straightforward to formulate and has already been discussed in some detail in [21]. The other one is the background field method described in appendix A which is used in the off-shell matching calculation. The additional Feynman rules that we need in the present paper, namely those involving photons and gluons, are collected in appendix B.

Here we only recall the most important features of the ACD model. The fifth dimension is compactified on the orbifold  $S^1/Z_2$  to reproduce chiral fermions in 4 dimensions. In addition to the ordinary particles of the SM, denoted as zero modes ( $n = 0$ ), there are infinite towers of KK modes ( $n \geq 1$ ). There is one such tower for each SM boson and two for each SM fermion, while there also exist physical scalars  $a_{(n)}^0$  and  $a_{(n)}^\pm$  with ( $n \geq 1$ ) that do not have any zero mode partners. The masses of the KK particles are universally given by

$$m_{(n)}^2 = m_0^2 + \frac{n^2}{R^2}. \quad (2.1)$$

Here  $m_0$  is the mass of the zero mode, as  $M_W$ ,  $M_Z$ ,  $m_t$ . For  $a_{(n)}^0$  and  $a_{(n)}^\pm$  this is  $M_Z$  and  $M_W$ , respectively. The compactification radius  $R$  is the only additional parameter relative to the SM. To a quark  $SU(2)_L$  doublet, there correspond the KK modes  $\mathcal{Q}$ , whereas the partners of the right-handed singlets are  $\mathcal{U}$  and  $\mathcal{D}$ .

As the KK modes contribute to the process considered here first at the one loop level, the natural variables that enter the Inami-Lim functions are

$$x_{i(n)} = \frac{m_{i(n)}^2}{M_{W(n)}^2} \quad (2.2)$$

with  $m_{i(n)}$  denoting the masses of the fermionic KK modes and  $M_{W(n)}$  the masses of the  $W$  boson KK modes. However, in phenomenological applications it is more useful to work with the variables  $x_t$  and  $x_n$  defined through

$$x_t = \frac{m_t^2}{M_W^2}, \quad x_n = \frac{m_n^2}{M_W^2}, \quad m_n = \frac{n}{R} \quad (2.3)$$

than with  $x_{i(n)}$ .

### 3 Penguin Diagrams in the ACD Model

#### 3.1 Preliminaries

The rare decays in the ACD model considered here are governed as in the SM by various penguin diagrams. The SM contributions to  $\Delta F = 1$  box diagrams are subleading but non-negligible. On the other hand the KK contributions to the latter diagrams are tiny [1] and can be neglected.

The penguin vertices including electroweak counter terms can be conveniently expressed in terms of the functions  $C$  ( $Z^0$  penguins),  $D$  ( $\gamma$  penguins),  $E$  (gluon penguins),  $D'$  ( $\gamma$ -magnetic penguins) and  $E'$  (chromomagnetic penguins). In the 't Hooft–Feynman gauge for the  $W^\pm$  and  $G^\pm$  propagators they are given as follows:

$$\bar{s}Zd = i\lambda_t \frac{G_F}{\sqrt{2}} \frac{g_2}{2\pi^2} \frac{M_W^2}{\cos\theta_w} C(x_t, 1/R) \bar{s}\gamma_\mu(1 - \gamma_5)d \quad (3.1)$$

$$\bar{s}\gamma d = -i\lambda_t \frac{G_F}{\sqrt{2}} \frac{e}{8\pi^2} D(x_t, 1/R) \bar{s}(q^2\gamma_\mu - q_\mu \not{q})(1 - \gamma_5)d \quad (3.2)$$

$$\bar{s}G^a d = -i\lambda_t \frac{G_F}{\sqrt{2}} \frac{g_s}{8\pi^2} E(x_t, 1/R) \bar{s}_\alpha(q^2\gamma_\mu - q_\mu \not{q})(1 - \gamma_5)T_{\alpha\beta}^a d_\beta \quad (3.3)$$

$$\bar{s}\gamma' b = i\bar{\lambda}_t \frac{G_F}{\sqrt{2}} \frac{e}{8\pi^2} D'(x_t, 1/R) \bar{s}[i\sigma_{\mu\lambda}q^\lambda[m_b(1 + \gamma_5)]]b \quad (3.4)$$

$$\bar{s}G'^a b = i\bar{\lambda}_t \frac{G_F}{\sqrt{2}} \frac{g_s}{8\pi^2} E'(x_t, 1/R) \bar{s}_\alpha[i\sigma_{\mu\lambda}q^\lambda[m_b(1 + \gamma_5)]]T_{\alpha\beta}^a b_\beta, \quad (3.5)$$

where  $G_F$  is the Fermi constant,  $\theta_w$  is the weak mixing angle and

$$\lambda_t = V_{ts}^* V_{td}, \quad \bar{\lambda}_t = V_{ts}^* V_{tb}. \quad (3.6)$$

In these vertices  $q_\mu$  is the *outgoing* gluon or photon momentum and  $T^a$  are colour matrices. The last two vertices involve on-shell photon and gluon, respectively. We have set  $m_s = 0$  in these vertices.

Each function in (3.1)–(3.5) is given by

$$F(x_t, 1/R) = F_0(x_t) + \sum_{n=1}^{\infty} F_n(x_t, x_n), \quad F = C, D, E, D', E', \quad (3.7)$$

with  $x_n$  defined in (2.3). The functions  $F_n(x_t, x_n)$  in (3.7) are defined through

$$F_n(x_t, x_n) = G(x_{t(n)}) - G(x_{u(n)}), \quad (3.8)$$

with  $x_{i(n)}$  defined in (2.2) and the functions  $G(x_{t(n)})$  and  $G(x_{u(n)})$  representing the contributions of the  $\mathcal{Q}_{t(n)}$ ,  $\mathcal{U}_{t(n)}$  and  $\mathcal{Q}_{u(n)}$ ,  $\mathcal{U}_{u(n)}$  modes, respectively.

The functions  $F_0(x_t)$  result from the penguin diagrams in the SM and the sum represents the KK contributions to the relevant penguin diagrams.  $F_0(x_t)$  were calculated by various authors, in particular by Inami and Lim [18]. They are given explicitly as follows:

$$C_0(x_t) = \frac{x_t}{8} \left[ \frac{x_t - 6}{x_t - 1} + \frac{3x_t + 2}{(x_t - 1)^2} \ln x_t \right], \quad (3.9)$$

$$D_0(x_t) = -\frac{4}{9} \ln x_t + \frac{-19x_t^3 + 25x_t^2}{36(x_t - 1)^3} + \frac{x_t^2(5x_t^2 - 2x_t - 6)}{18(x_t - 1)^4} \ln x_t, \quad (3.10)$$

$$E_0(x_t) = -\frac{2}{3} \ln x_t + \frac{x_t^2(15 - 16x_t + 4x_t^2)}{6(1 - x_t)^4} \ln x_t + \frac{x_t(18 - 11x_t - x_t^2)}{12(1 - x_t)^3}, \quad (3.11)$$

$$D'_0(x_t) = -\frac{(8x_t^3 + 5x_t^2 - 7x_t)}{12(1 - x_t)^3} + \frac{x_t^2(2 - 3x_t)}{2(1 - x_t)^4} \ln x_t, \quad (3.12)$$

$$E'_0(x_t) = -\frac{x_t(x_t^2 - 5x_t - 2)}{4(1 - x_t)^3} + \frac{3}{2} \frac{x_t^2}{(1 - x_t)^4} \ln x_t. \quad (3.13)$$

The  $Z^0$  penguin functions  $C_n(x_t, x_n)$  have been calculated in [1] with the result

$$C_n(x_t, x_n) = \frac{x_t}{8(x_t - 1)^2} \left[ x_t^2 - 8x_t + 7 + (3 + 3x_t + 7x_n - x_t x_n) \ln \frac{x_t + x_n}{1 + x_n} \right]. \quad (3.14)$$

In the present paper we will calculate the remaining functions  $D_n(x_t, x_n)$ ,  $E_n(x_t, x_n)$ ,  $D'_n(x_t, x_n)$  and  $E'_n(x_t, x_n)$ .

### 3.2 General Structure of the Calculation

The function  $F_n(x_t, x_n)$  with  $F = D, E, D', E'$  can be found by calculating the vertex diagrams in fig. 1. Contrary to the  $Z^0$  penguins where one has to add an electroweak counter term as discussed in [22], this is not necessary for the  $\gamma$  and gluon penguins. Here the counter terms are only formally used to render zero the coefficients of the dimension 4 operators  $\bar{s}A P_L q$  and  $\bar{s}T^a Q^a P_L q$  with  $q = d, b$ . This is a consequence of gauge invariance when the quark fields are set on-shell with the renormalization condition given in [23].

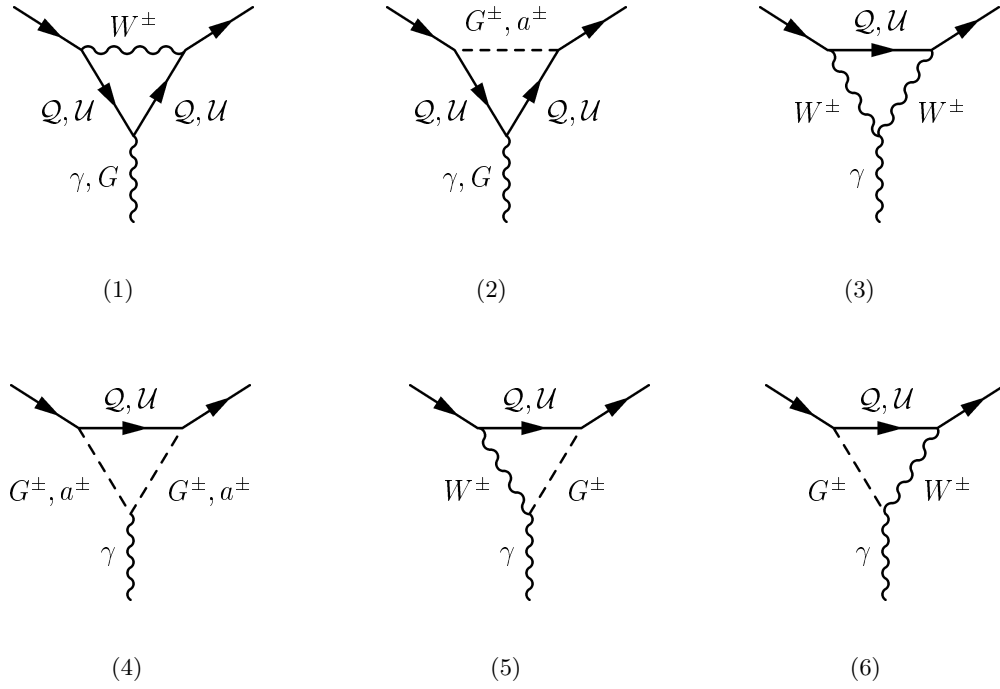


Figure 1: Penguin diagrams contributing to  $F_n(x_t, x_n)$ .

In contrast to the calculation of the  $Z^0$ -vertex the external momenta in fig. 1 and the masses of external quarks cannot be neglected.

The calculation of the functions  $F$  was done in two different ways. The common starting point is the effective Hamiltonian at the matching scale  $\mu_W$

$$\mathcal{H}_{\text{eff}}(b \rightarrow s\gamma, G) = -\frac{G_F}{\sqrt{2}} V_{ts}^* V_{tb} \left[ \sum_{i=30}^{36} C_i(\mu_W) Q_i + C_{7\gamma}(\mu_W) Q_{7\gamma} + C_{8G}(\mu_W) Q_{8G} \right], \quad (3.15)$$

with the operators [24]

$$Q_{7\gamma} = \frac{e}{4\pi^2} m_b (\bar{s} \sigma_{\mu\nu} P_R b) F^{\mu\nu}, \quad (3.16)$$

$$Q_{8G} = \frac{g_s}{4\pi^2} m_b (\bar{s} \sigma_{\mu\nu} P_R \mathbf{T}^a b) G^{a,\mu\nu}, \quad (3.17)$$

$$Q_{30} = \frac{i}{4\pi^2} M_W^2 (\bar{s} \not{D} P_L b), \quad (3.18)$$

$$Q_{31} = \frac{g_s}{4\pi^2} (\bar{s} P_R \gamma_\mu \mathbf{T}^a b) D_\nu G^{a,\mu\nu} + Q_4, \quad (3.19)$$

$$Q_{32} = \frac{1}{4\pi^2} m_b (\bar{s} P_R \not{D} \not{D} b), \quad (3.20)$$

$$Q_{33} = \frac{i}{4\pi^2} (\bar{s} P_R \not{D} \not{D} \not{D} b), \quad (3.21)$$

$$Q_{34} = \frac{ig_s}{4\pi^2} \bar{s} P_R \left[ \overleftarrow{\not{D}} \sigma_{\mu\nu} \mathbf{T}^a - \mathbf{T}^a \sigma_{\mu\nu} (\not{D} + im_b) \right] b G^{a,\mu\nu}, \quad (3.22)$$

$$Q_{35} = \frac{ie}{4\pi^2} \bar{s} P_R \left[ \overleftarrow{\not{D}} \sigma_{\mu\nu} - \sigma_{\mu\nu} (\not{D} + im_b) \right] b F^{\mu\nu}, \quad (3.23)$$

$$Q_{36} = \frac{e}{4\pi^2} (\bar{s} P_R \gamma_\mu b) \partial_\nu F^{\mu\nu} - Q_9. \quad (3.24)$$

The covariant derivative in the effective Lagrangian is defined as<sup>1</sup>

$$D_\mu \psi = (\partial_\mu + ie Q_\psi A_\mu + ig_s \mathbf{T}^a G_\mu^a) \psi. \quad (3.25)$$

In the operators  $Q_{34}$  and  $Q_{35}$  it acts only on the spinors, but not on the field strength tensors  $F^{\mu\nu}$  and  $G^{a,\mu\nu}$ .

In this off-shell operator basis we have omitted the four-quark operators as they are not relevant for the calculation of the functions  $F$ . They can be found in [24], in particular the operators  $Q_4$  and  $Q_9$  that appear in the definition of  $Q_{31}$  and  $Q_{36}$ . The effective vertices (3.2)-(3.5) correspond to the operators  $Q_{36}$ ,  $Q_{31}$ ,  $Q_{7\gamma}$  and  $Q_{8G}$ , respectively.

In the first method the equations of motion of the quark fields and the relation  $q^2 = 0$  are applied both on the full and on the effective side of the matching amplitude. After renormalization the amplitude on the effective side is

$$\mathcal{A}_{\text{eff}}^{b \rightarrow s\gamma} = \bar{\lambda}_t \frac{G_F}{\sqrt{2}} \frac{ie}{8\pi^2} \bar{s} [D'(2T_1 + T_2) - DT_2] b \quad (3.26)$$

with  $T_1 = m_b \not{q} \gamma_\mu P_R$  and  $T_2 = -2m_b q_\mu P_R$ .

The full side was evaluated with the Feynman diagrams (1)-(6) in fig. 1 in 't Hooft-Feynman gauge. The vertices  $A_{(0)} W_{(n)}^\pm a_{(n)}^\mp$  and  $A_{(0)} G_{(n)}^\pm a_{(n)}^\mp$  are zero, hence there are no diagrams with these vertices to be considered. The result can be written as

$$\mathcal{A}_{\text{full}}^{b \rightarrow s\gamma} = \bar{\lambda}_t \frac{G_F}{\sqrt{2}} \frac{ie}{8\pi^2} \bar{s} [H_1 T_1 + H_2 T_2] b, \quad (3.27)$$

yielding

$$D = \frac{1}{2} H_1 - H_2, \quad D' = \frac{1}{2} H_1. \quad (3.28)$$

---

<sup>1</sup>On the effective side we use a different sign convention for the couplings  $e$  and  $g_s$  compared to the Feynman rules in this paper and in [1].

For the functions  $E$  and  $E'$  the procedure is analogous. As the gluon couples only to the quarks the relevant diagrams in this case are (1) and (2).

The second method uses the off-shell amplitude for the matching, i.e. no equations of motion are applied. In order to maintain gauge invariance the method of background fields [25] is used. Here the matching is done with the full set of operators (3.16)-(3.24).

For the full side the diagrams (1)-(4) in fig. 1 were evaluated in 't Hooft-Feynman gauge with the Feynman rules for the background fields  $\hat{\gamma}$  and  $\hat{G}$  given in appendix B. As a virtue of the background field (BF) method, the diagrams (5) and (6) do not show up because the vertex  $\hat{A}_{(0)}W_{(n)}^\pm G_{(n)}^\mp$  vanishes.

The effective side can be directly matched to the full side. Comparing (3.2)-(3.5) with (3.15) we can read off

$$D = -C_{36}^{(0)}(\mu_W), \quad D' = -2C_{7\gamma}^{(0)}(\mu_W), \quad (3.29)$$

$$E = -C_{31}^{(0)}(\mu_W), \quad E' = -2C_{8G}^{(0)}(\mu_W), \quad (3.30)$$

where “(0)” indicates the leading coefficients without QCD corrections. We found the same results for the functions  $F$  with both methods.

### 3.3 The functions $D$ , $E$ , $D'$ , $E'$ and $Z$

Adding up the contributions from the diagrams of fig. 1 we find

$$\begin{aligned} D_n(x_t, x_n) &= \frac{x_t (35 + 8x_t - 19x_t^2 + 6x_n^2 (10 - 9x_t + 3x_t^2)) + 3x_n (53 - 58x_t + 21x_t^2)}{108(x_t - 1)^3} \\ &\quad + \frac{1}{6} (4 - 2x_n + 4x_n^2 + x_n^3) \ln \frac{x_n}{1 + x_n} \\ &\quad - \frac{1}{18(x_t - 1)^4} (12 - 38x_t + 54x_t^2 - 27x_t^3 + 3x_t^4 + x_n^3 (3 + x_t) + 3x_n^2 (4 - x_t + x_t^2)) \\ &\quad + x_n (-6 + 42x_t - 33x_t^2 + 9x_t^3) \ln \frac{x_n + x_t}{1 + x_n}, \end{aligned} \quad (3.31)$$

$$\begin{aligned} E_n(x_t, x_n) &= -\frac{x_t (35 + 8x_t - 19x_t^2 + 6x_n^2 (10 - 9x_t + 3x_t^2)) + 3x_n (53 - 58x_t + 21x_t^2)}{36(x_t - 1)^3} \\ &\quad - \frac{1}{2} (1 + x_n) (-2 + 3x_n + x_n^2) \ln \frac{x_n}{1 + x_n} \\ &\quad + \frac{(1 + x_n) (-6 + 19x_t - 9x_t^2 + x_n^2 (3 + x_t) + x_n (9 - 4x_t + 3x_t^2))}{6(x_t - 1)^4} \ln \frac{x_n + x_t}{1 + x_n}, \end{aligned} \quad (3.32)$$

$$\begin{aligned}
D'_n(x_t, x_n) = & \frac{x_t (-37 + 44x_t + 17x_t^2 + 6x_n^2 (10 - 9x_t + 3x_t^2)) - 3x_n (21 - 54x_t + 17x_t^2)}{36(-1 + x_t)^3} \\
& + \frac{x_n (2 - 7x_n + 3x_n^2)}{6} \ln \frac{x_n}{1 + x_n} \\
& - \frac{(-2 + x_n + 3x_t) (x_t + 3x_t^2 + x_n^2 (3 + x_t) - x_n (1 + (-10 + x_t) x_t))}{6(-1 + x_t)^4} \ln \frac{x_n + x_t}{1 + x_t}, \quad (3.33)
\end{aligned}$$

$$\begin{aligned}
E'_n(x_t, x_n) = & \frac{x_t (-17 - 8x_t + x_t^2 - 3x_n (21 - 6x_t + x_t^2)) - 6x_n^2 (10 - 9x_t + 3x_t^2)}{12(x_t - 1)^3} \\
& - \frac{1}{2} x_n (1 + x_n) (-1 + 3x_n) \ln \frac{x_n}{1 + x_n} \\
& + \frac{(1 + x_n) (x_t + 3x_t^2 + x_n^2 (3 + x_t) - x_n (1 + (-10 + x_t) x_t))}{2(x_t - 1)^4} \ln \frac{x_n + x_t}{1 + x_n}. \quad (3.34)
\end{aligned}$$

In fig. 2 we plot the functions  $F(x_t, 1/R)$  versus  $1/R$ . The impact of the KK modes on the function  $D$  is negligible. The function  $E$  is moderately enhanced but this enhancement plays only a marginal role in our phenomenological applications. The most interesting are very strong suppressions of  $D'$  and  $E'$ , that for  $1/R = 300$  GeV amount to 36% and 66% relative to the SM values, respectively.

While the  $\Delta F = 2$  box function  $S$  and the penguin functions  $E$ ,  $D'$  and  $E'$  are gauge independent, this is not the case for  $C$ ,  $D$  and the  $\Delta F = 1$  box diagram functions  $B^{\nu\bar{\nu}}$  and  $B^{\mu\bar{\mu}}$  considered in [1]. In phenomenological applications it is more convenient to work with gauge independent functions [20]

$$X(x_t, 1/R) = C(x_t, 1/R) + B^{\nu\bar{\nu}}(x_t, 1/R) = X_0(x_t) + \Delta X, \quad (3.35)$$

$$Y(x_t, 1/R) = C(x_t, 1/R) + B^{\mu\bar{\mu}}(x_t, 1/R) = Y_0(x_t) + \Delta Y, \quad (3.36)$$

$$Z(x_t, 1/R) = C(x_t, 1/R) + \frac{1}{4}D(x_t, 1/R) = Z_0(x_t) + \Delta Z \quad (3.37)$$

with ( $m_t = 167$  GeV)

$$X_0(x_t) = \frac{x_t}{8} \left[ \frac{x_t + 2}{x_t - 1} + \frac{3x_t - 6}{(x_t - 1)^2} \ln x_t \right] = 1.526, \quad (3.38)$$

$$Y_0(x_t) = \frac{x_t}{8} \left[ \frac{x_t - 4}{x_t - 1} + \frac{3x_t}{(x_t - 1)^2} \ln x_t \right] = 0.980 \quad (3.39)$$

$$\begin{aligned}
Z_0(x_t) = & -\frac{1}{9} \ln x_t + \frac{18x_t^4 - 163x_t^3 + 259x_t^2 - 108x_t}{144(x_t - 1)^3} + \\
& + \frac{32x_t^4 - 38x_t^3 - 15x_t^2 + 18x_t}{72(x_t - 1)^4} \ln x_t = 0.679 \quad (3.40)
\end{aligned}$$

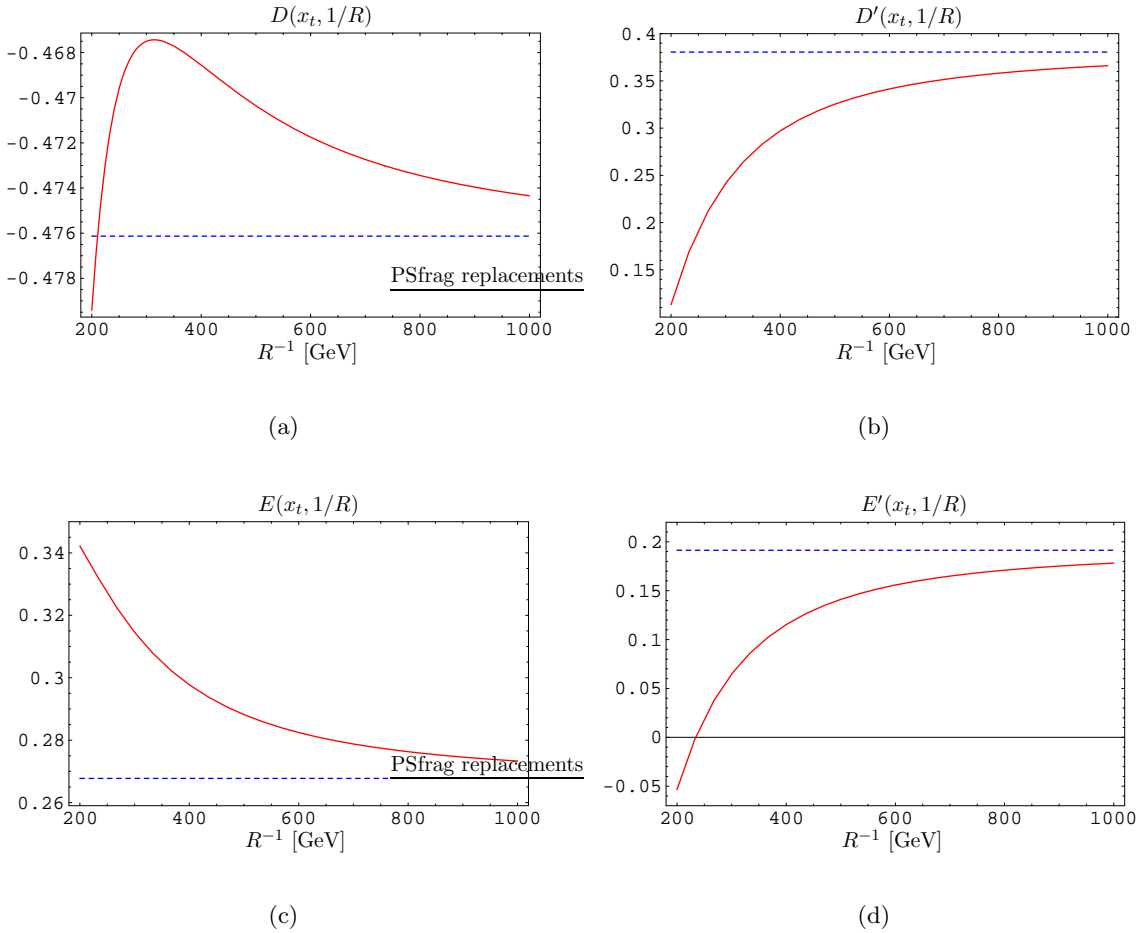


Figure 2: The functions  $F(x_t, 1/R)$  and  $F_0(x_t)$  with  $F = D, E, D', E'$  plotted versus  $1/R$ . The constant dashed lines are the SM values.

summarizing the SM contributions and  $\Delta X$ ,  $\Delta Y$  and  $\Delta Z$  representing the corrections due to KK modes. Our analysis of [1] and the negligible KK contributions to the function  $D$  found here imply to an excellent approximation

$$\Delta X = \Delta Y = \Delta Z = \sum_{n=1}^{\infty} C_n(x_t, x_n). \quad (3.41)$$

In table 1 we give the values of the gauge independent functions  $S$ ,  $X$ ,  $Y$  calculated in [1] and of  $Z$ ,  $E$ ,  $D'$ ,  $E'$  calculated here for different  $1/R$  and  $m_t = 167$  GeV. Our results for the function  $S$  have been confirmed in [26]. For completeness we give also the values of  $C$  and  $D$  in 't Hooft–Feynman gauge. We observe that for  $1/R = 300$  GeV, the functions  $X$ ,  $Y$ ,  $Z$  are enhanced by 10%, 15% and 23% relative to the SM values, respectively. While these enhancements are smaller than the corresponding suppressions of  $D'$  and  $E'$ , the effect of the latter suppressions

will be softened in the relevant branching ratios through sizable additive QCD corrections.

$1/R$ [GeV]	$S$	$X$	$Y$	$Z$	$E$	$D'$	$E'$	$C$	$D$
200	2.813	1.826	1.281	0.990	0.342	0.113	-0.053	1.099	-0.479
250	2.664	1.731	1.185	0.893	0.327	0.191	0.019	1.003	-0.470
300	2.582	1.674	1.128	0.835	0.315	0.242	0.065	0.946	-0.468
400	2.500	1.613	1.067	0.771	0.298	0.297	0.115	0.885	-0.469
SM	2.398	1.526	0.980	0.679	0.268	0.380	0.191	0.798	-0.476

Table 1: Values for the functions  $S, X, Y, Z, E, D', E', C$  and  $D$ .

## 4 $B \rightarrow X_s \gamma$

### 4.1 Preliminaries

The inclusive  $B \rightarrow X_s \gamma$  decay has been the subject of very intensive theoretical and experimental studies during the last 15 years. On the experimental side the world average resulting from the data by CLEO, ALEPH, BaBar and Belle reads [27]

$$Br(B \rightarrow X_s \gamma)_{E_\gamma > 1.6 \text{ GeV}} = (3.28^{+0.41}_{-0.36}) \cdot 10^{-4} . \quad (4.1)$$

It agrees well with the SM result [28, 29]

$$Br(B \rightarrow X_s \gamma)_{E_\gamma > 1.6 \text{ GeV}}^{\text{SM}} = (3.57 \pm 0.30) \cdot 10^{-4} . \quad (4.2)$$

The most recent reviews summarizing the theoretical status can be found in [30, 31, 32]. The purpose of this section is the calculation of the impact of the KK modes on the branching ratio in question.

As the NLO QCD corrections to  $Br(B \rightarrow X_s \gamma)$  within the SM are very important, it is mandatory to include them also in the ACD model. Fortunately, the QCD corrections for scales  $\mu < 1/R$  are in the ACD model precisely the same as in the SM and the only elements of the NLO QCD corrections to  $Br(B \rightarrow X_s \gamma)$  within the ACD model that are missing, are the  $\mathcal{O}(\alpha_s)$  corrections to the functions  $D'$  and  $E'$ . The experience with such corrections within the SM and MSSM at low  $\tan\beta$  makes us to expect that they are significantly smaller than the renormalization group effects for  $\mu < M_W$  and the  $\mathcal{O}(\alpha_s)$  corrections at scales  $\mathcal{O}(m_b)$ . Therefore we are confident that it is a good approximation to neglect these corrections in the case of the KK contributions.

Now, the NLO formulae for the relevant Wilson coefficients and the  $Br(B \rightarrow X_s \gamma)$  are very complicated and not transparent. Therefore we will first discuss the impact of the KK contributions at the LO level. Subsequently we will present the numerical results of an NLO analysis that uses the formulae of [28] modified by the KK contributions to the functions  $D'$  and  $E'$  calculated in the previous section.

## 4.2 Effective Hamiltonian

The effective Hamiltonian for  $B \rightarrow X_s \gamma$  at scales  $\mu_b = \mathcal{O}(m_b)$  is given by

$$\mathcal{H}_{\text{eff}}(b \rightarrow s \gamma) = -\frac{G_F}{\sqrt{2}} V_{ts}^* V_{tb} \left[ \sum_{i=1}^6 C_i(\mu_b) Q_i + C_{7\gamma}(\mu_b) Q_{7\gamma} + C_{8G}(\mu_b) Q_{8G} \right], \quad (4.3)$$

where in view of  $|V_{us}^* V_{ub}/V_{ts}^* V_{tb}| < 0.02$  we have neglected the term proportional to  $V_{us}^* V_{ub}$ . Here  $Q_1 \dots Q_6$  are the usual four-quark operators whose explicit form can be found in [33]. The remaining two operators, characteristic for this decay, are the *magnetic-penguins*

$$Q_{7\gamma} = \frac{e}{8\pi^2} m_b \bar{s}_\alpha \sigma^{\mu\nu} (1 + \gamma_5) b_\alpha F_{\mu\nu}, \quad Q_{8G} = \frac{g_s}{8\pi^2} m_b \bar{s}_\alpha \sigma^{\mu\nu} (1 + \gamma_5) T_{\alpha\beta}^a b_\beta G_{\mu\nu}^a \quad (4.4)$$

originating in the diagrams of fig. 1 with on-shell photon and gluon, respectively.

The coefficients  $C_i(\mu_b)$  in (4.3) can be calculated by using

$$C(\mu_b) = \hat{U}_5(\mu_b, \mu_W) C(\mu_W) \quad (4.5)$$

Here  $\hat{U}_5(\mu_b, \mu_W)$  with  $\mu_W = \mathcal{O}(M_W)$  is the  $8 \times 8$  evolution matrix that is known including NLO corrections [34]. As stated before, we will first estimate the effect of the KK modes on  $C_{7\gamma}(\mu_b)$  and  $C_{8G}(\mu_b)$  in the leading logarithmic (LO) approximation. In this case generalizing the SM formulae in [35] to the ACD model we obtain

$$C_{7\gamma}^{(0)eff}(\mu_b) = \eta^{\frac{16}{23}} C_{7\gamma}^{(0)}(\mu_W) + \frac{8}{3} \left( \eta^{\frac{14}{23}} - \eta^{\frac{16}{23}} \right) C_{8G}^{(0)}(\mu_W) + C_2^{(0)}(\mu_W) \sum_{i=1}^8 h_i \eta^{a_i}, \quad (4.6)$$

$$C_{8G}^{(0)eff}(\mu_b) = \eta^{\frac{14}{23}} C_{8G}^{(0)}(\mu_W) + C_2^{(0)}(\mu_W) \sum_{i=1}^8 \bar{h}_i \eta^{a_i}, \quad (4.7)$$

with

$$\eta = \frac{\alpha_s(\mu_W)}{\alpha_s(\mu_b)}, \quad (4.8)$$

and

$$C_2^{(0)}(\mu_W) = 1, \quad C_{7\gamma}^{(0)}(\mu_W) = -\frac{1}{2} D'(x_t, 1/R), \quad C_{8G}^{(0)}(\mu_W) = -\frac{1}{2} E'(x_t, 1/R) \quad (4.9)$$

and all remaining coefficients equal zero at  $\mu = \mu_W$ . The superscript “0” indicates the LO approximation. The “effective” coefficients in (4.6) and (4.7) are introduced in place of  $C_{7\gamma}(\mu_b)$  and  $C_{8G}(\mu_b)$  in order to keep the LO Wilson coefficients renormalization scheme independent as discussed in [35]. The functions  $D'(x_t, 1/R)$  and  $E'(x_t, 1/R)$  have been calculated in section 3. Finally the values of  $a_i$ ,  $h_i$  and  $\bar{h}_i$  are given in table 2.

$i$	1	2	3	4	5	6	7	8
$a_i$	$\frac{14}{23}$	$\frac{16}{23}$	$\frac{6}{23}$	$-\frac{12}{23}$	0.4086	-0.4230	-0.8994	0.1456
$h_i$	2.2996	-1.0880	$-\frac{3}{7}$	$-\frac{1}{14}$	-0.6494	-0.0380	-0.0185	-0.0057
$\bar{h}_i$	0.8623	0	0	0	-0.9135	0.0873	-0.0571	0.0209

Table 2: Magic Numbers.

Using the leading  $\mu_b$ -dependence of  $\alpha_s$  in an effective five quark theory

$$\alpha_s^{(5)}(\mu_b) = \frac{\alpha_s(M_Z)}{1 - \beta_0 \frac{\alpha_s(M_Z)}{2\pi} \ln(M_Z/\mu_b)}, \quad \beta_0 = \frac{23}{3}, \quad (4.10)$$

and setting  $\alpha_s^{(5)}(M_Z) = 0.118$  we find the results in table 3.

	$\mu_b = 2.5 \text{ GeV}$		$\mu_b = 5.0 \text{ GeV}$		$\mu_b = 7.5 \text{ GeV}$	
$1/R[\text{GeV}]$	$C_{7\gamma}^{(0)\text{eff}}$	$C_{8G}^{(0)\text{eff}}$	$C_{7\gamma}^{(0)\text{eff}}$	$C_{8G}^{(0)\text{eff}}$	$C_{7\gamma}^{(0)\text{eff}}$	$C_{8G}^{(0)\text{eff}}$
200	-0.236	-0.076	-0.192	-0.053	-0.169	-0.040
250	-0.264	-0.100	-0.223	-0.079	-0.201	-0.068
300	-0.282	-0.114	-0.242	-0.096	-0.221	-0.086
400	-0.301	-0.131	-0.264	-0.114	-0.244	-0.105
SM	-0.331	-0.156	-0.296	-0.142	-0.278	-0.135

Table 3: Wilson coefficients  $C_{7\gamma}^{(0)\text{eff}}$  and  $C_{8G}^{(0)\text{eff}}$  in LO for  $m_t = 167 \text{ GeV}$  as functions of  $1/R$  and various values of  $\mu_b$ .

We observe a sizable impact of the KK modes on the coefficients  $C_{7\gamma}^{(0)\text{eff}}(\mu_b)$  and  $C_{8G}^{(0)\text{eff}}(\mu_b)$  although this impact is substantially smaller than on  $C_{7\gamma}^{(0)}(\mu_W)$  and  $C_{8G}^{(0)}(\mu_W)$  in (4.9). This can be understood by investigating the size of the different terms in (4.6) and (4.7). Setting  $m_t = 167 \text{ GeV}$ ,  $1/R = 300 \text{ GeV}$ ,  $\mu_b = 5 \text{ GeV}$  and  $\alpha_s^{(5)}(M_Z) = 0.118$  we find

$$\begin{aligned} C_{7\gamma}^{(0)\text{eff}}(\mu_b) &= 0.695 C_{7\gamma}^{(0)}(\mu_W) + 0.085 C_{8G}^{(0)}(\mu_W) - 0.158 C_2^{(0)}(\mu_W) \\ &= 0.695 (-0.121) + 0.085 (-0.033) - 0.158 = -0.245 \end{aligned} \quad (4.11)$$

to be compared with  $-0.300$  in the SM. In the absence of QCD corrections we would have  $C_{7\gamma}^{(0)\text{eff}}(\mu_b) = C_{7\gamma}^{(0)}(\mu_W)$  (in that case one has  $\eta = 1$ ) and the KK effects would be very large as found in section 3. However, the additive QCD correction present in the last term in (4.11) that causes the large QCD enhancement of the  $B \rightarrow X_s\gamma$  [36, 37] screens considerably the effects of the KK modes. Similar comments apply to  $C_{8G}^{(0)\text{eff}}$  for which we find

$$\begin{aligned} C_{8G}^{(0)\text{eff}}(\mu_b) &= 0.727 C_{8G}^{(0)}(\mu_W) - 0.074 C_2^{(0)}(\mu_W) \\ &= 0.727 (-0.033) - 0.074 = -0.098 \end{aligned} \quad (4.12)$$

to be compared with  $-0.144$  in the SM.

We also observe that the strong  $\mu_b$ -dependence of both coefficients [38, 35] is large. This scale-uncertainty in the leading order can be substantially reduced by including NLO corrections.

### 4.3 The Branching Ratio

In the leading logarithmic approximation one has

$$\frac{Br(B \rightarrow X_s\gamma)}{Br(B \rightarrow X_c e \bar{\nu}_e)} = \frac{|V_{ts}^* V_{tb}|^2}{|V_{cb}|^2} \frac{6\alpha}{\pi f(z)} |C_7^{(0)\text{eff}}(\mu_b)|^2, \quad (4.13)$$

where  $f(z)$  with  $z = m_c/m_b$  is the phase space factor in  $Br(B \rightarrow X_c e \bar{\nu}_e)$ .

The corresponding NLO formulae that include also higher order electroweak effects [39] are very complicated and can be found in [28]. As reviewed in [30, 31, 32], many groups contributed to obtain these NLO results. In our numerical NLO analysis we benefited enormously from the computer programs of the authors of [28, 39].

In table 4 we show the results for  $Br(B \rightarrow X_s\gamma)$  at LO and NLO for the central values of the input parameters in [28] and different values of  $\mu_b$ . While in the LO the  $\mu_b$  dependence is very sizable, it is very small after including NLO corrections. The strong enhancement of the branching ratio by additive QCD corrections calculated first in [40] and confirmed in [29] is particularly visible at low  $1/R$  for which the Wilson coefficients of the magnetic operators are strongly suppressed by the KK modes and the additive QCD corrections become even more important than in the SM. This table demonstrates very clearly the importance of higher order QCD calculations in the search for new physics. Without them any comparison between the SM, the ACD model and the experimental data would be meaningless.

The strong suppression of the branching ratio by the KK modes is clearly seen. In fig. 3 we compare  $Br(B \rightarrow X_s\gamma)$  in the ACD model with the experimental data and with the expectations of the SM. The shaded region represents the data in (4.1) and the upper (lower) dashed horizontal line are the central values in the SM for  $m_c/m_b = 0.22$  ( $m_c/m_b = 0.29$ ). The solid lines represent

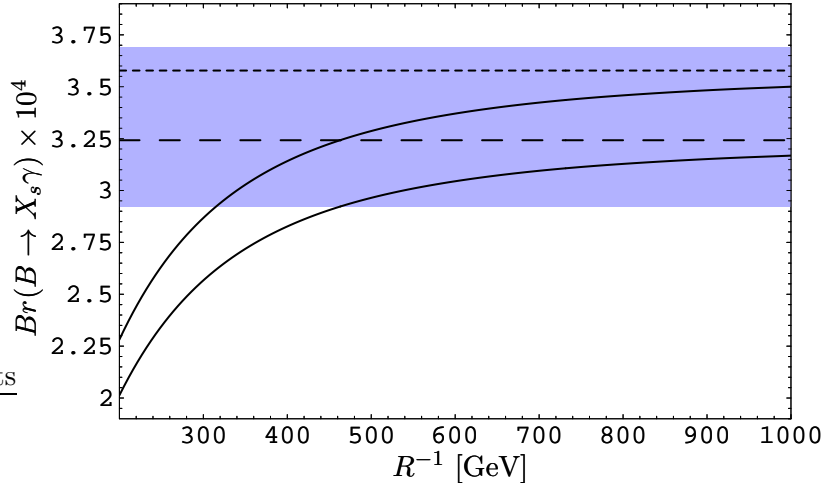


Figure 3: The branching ratio for  $B \rightarrow X_s \gamma$  and  $E_\gamma > 1.6$  GeV as a function of  $1/R$ . See text for the meaning of various curves.

the corresponding central values in the ACD model. The theoretical errors, not shown in the plot, are for all curves roughly  $\pm 10\%$ .

We observe that in view of the sizable experimental error and considerable parametric uncertainties in the theoretical prediction, the strong suppression of  $Br(B \rightarrow X_s \gamma)$  by the KK modes does not yet provide a powerful lower bound on  $1/R$  and the values  $1/R \geq 250$  GeV are fully consistent with the experimental result. It should also be emphasized that  $Br(B \rightarrow X_s \gamma)$  depends sensitively on the ratio  $m_c/m_b$  that in (4.2) and table 4 has been set to 0.22 in accordance with the arguments put forward in [28]. As seen in fig. 3, for a value  $m_c/m_b = 0.29$  that has been used in the past, the branching ratio is smaller by roughly 10% and the lower bound on  $1/R$  is shifted above 400 GeV if other uncertainties are neglected. In order to reduce the dependence on  $m_c/m_b$  a NNLO calculation is required. Once it is completed and the experimental uncertainties reduced,  $Br(B \rightarrow X_s \gamma)$  may provide a very powerful bound on  $1/R$  that is substantially stronger than the bounds obtained from the electroweak precision data.

The suppression of  $Br(B \rightarrow X_s \gamma)$  in the ACD model has already been found in [3]. Our result presented above is consistent with the one obtained by these authors but differs in details as only the dominant diagrams have been taken into account in the latter paper and the analysis was performed in the LO approximation.

1/R[GeV]	$\mu_b = 2.5 \text{ GeV}$		$\mu_b = 5.0 \text{ GeV}$		$\mu_b = 7.5 \text{ GeV}$	
	Br(LO)	Br(NLO)	Br(LO)	Br(NLO)	Br(LO)	Br(NLO)
200	1.54	2.32	1.02	2.30	0.79	2.28
250	1.92	2.66	1.37	2.65	1.11	2.63
300	2.18	2.89	1.61	2.88	1.35	2.86
400	2.49	3.15	1.90	3.15	1.63	3.13
SM	2.99	3.57	2.39	3.58	2.11	3.56

Table 4: The branching ratio for  $B \rightarrow X_s \gamma$  in LO and NLO in units of  $10^{-4}$  as a function of  $1/R$  for  $m_c/m_b = 0.22$  and various values of  $\mu_b$ .

## 5 $B \rightarrow X_s$ gluon

### 5.1 Preliminaries

The decay  $b \rightarrow sg$  is governed by the operator  $Q_{8G}$  and consequently the value of the coefficient  $C_{8G}$  is crucial here. In the SM the branching ratio for  $b \rightarrow sg$  is strongly enhanced by NLO QCD corrections [41] with the result

$$Br(b \rightarrow sg) = (5.0 \pm 1.0) \cdot 10^{-3}, \quad m_c/m_b = 0.29 \quad (5.1)$$

which is larger by a factor of 2.5 than the LO value. The sizable uncertainty shown in (5.1) is due solely to the renormalization scale dependence. The other important uncertainty is the value of  $m_c/m_b$ . For  $m_c/m_b = 0.22$  we find using the computer program of [41]

$$Br(b \rightarrow sg) = (4.1 \pm 0.7) \cdot 10^{-3}, \quad m_c/m_b = 0.22. \quad (5.2)$$

In fig. 4 we show the results for  $Br(b \rightarrow sg)$  in the ACD model as a function of  $1/R$  for three values of  $\mu_b$  and  $m_c/m_b = 0.22$ . In obtaining these results we benefited enormously from the computer program of the authors of [41]. As anticipated in section 3, there is a very strong suppression of the branching ratio in question by the KK contributions and if the strong  $\mu_b$  and  $m_c/m_b$  dependences could be put under control and the branching ratio could somehow be extracted from the data, the decay  $B \rightarrow X_s$  gluon could offer a very powerful constraint on  $1/R$ . Indeed, even for  $1/R = 600 \text{ GeV}$  a clear distinction between the SM and the ACD model predictions can be made for a fixed  $\mu_b$ .

Unfortunately, it will take some time before the strong  $\mu_b$  and  $m_c/m_b$  dependences can be significantly reduced and the extraction of the branching ratio from the experimental data is very difficult if not impossible [41, 42]. Yet, it is not excluded that one day this result could become relevant.

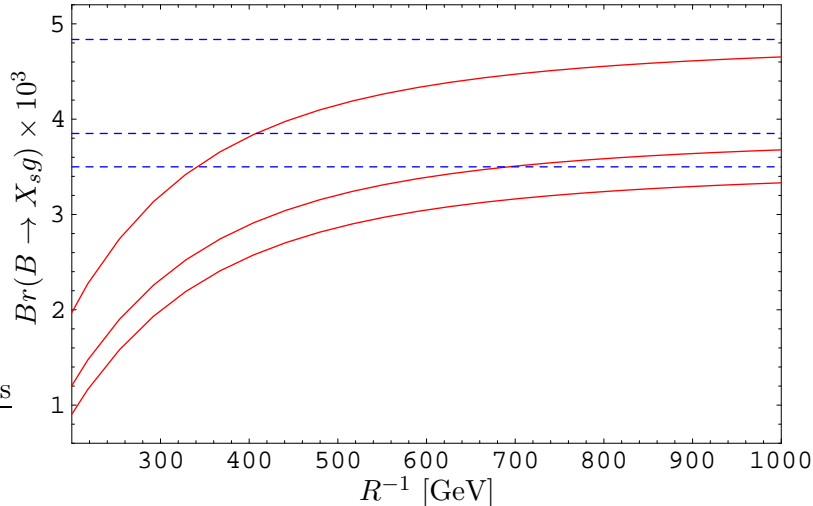


Figure 4: The branching ratio for  $B \rightarrow X_s g$  for  $m_c/m_b = 0.22$  and  $\mu_b = 2.5, 5, 7.5$  GeV.  $Br(B \rightarrow X_s g)$  decreases with increasing  $\mu_b$ . The dashed lines represent the SM prediction.

## 6 $B \rightarrow X_s \mu^+ \mu^-$

### 6.1 Preliminaries

The inclusive  $B \rightarrow X_s \mu^+ \mu^-$  decay has been the subject of very intensive theoretical and experimental studies during the last 15 years. On the experimental side only the BELLE collaboration reported the observation of this decay with [43]

$$Br(B \rightarrow X_s \mu^+ \mu^-) = (7.9 \pm 2.1_{-1.5}^{+2.0}) \cdot 10^{-6} . \quad (6.1)$$

For the decay to be dominated by perturbative contributions one has to remove  $\bar{c}c$  resonances by appropriate kinematical cuts in the dilepton mass spectrum. The SM expectation [44] for the low dilepton mass window is given by

$$\tilde{Br}(B \rightarrow X_s \mu^+ \mu^-)_{\text{SM}} = (2.75 \pm 0.45) \cdot 10^{-6} , \quad (6.2)$$

where the dilepton mass spectrum has been integrated in the limits suggested by BELLE [43] and given in (6.13).

This cannot be directly compared to the experimental result in (6.1) that is supposed to include the contributions from the full dilepton mass spectrum. Fortunately future experimental analyses are supposed to give the results corresponding to the low dilepton mass window so that a direct comparison between experiment and theory will be possible.

The most recent reviews summarizing the theoretical status can be found in [32, 44]. The purpose of this section is the calculation of the impact of the KK modes on the branching ratio, the invariant dilepton mass spectrum and the forward-backward asymmetry.

In contrast to the  $B \rightarrow X_s \gamma$  decay the inclusion of NLO corrections to  $Br(B \rightarrow X_s \mu^+ \mu^-)$  does not require the calculation of QCD corrections to the relevant penguin and box diagrams. Detailed explanation of this feature is given in [33, 32, 45]. Consequently in this decay we are in the position to present the complete NLO analysis in the ACD model. On the other hand the NNLO corrections to  $B \rightarrow X_s \mu^+ \mu^-$  have been calculated by now within the SM [24, 46, 47] and it will be of interest to include these corrections also in the ACD model following the philosophy as in the case of NLO corrections to  $B \rightarrow X_s \gamma$  and  $B \rightarrow X_s$  gluon decays. However, in order to see the impact of the KK modes on  $B \rightarrow X_s \mu^+ \mu^-$  in a transparent manner we will first present a NLO analysis of this decay.

## 6.2 Effective Hamiltonian

The effective Hamiltonian at scales  $\mu = O(m_b)$  is given by

$$\mathcal{H}_{\text{eff}}(b \rightarrow s \mu^+ \mu^-) = \mathcal{H}_{\text{eff}}(b \rightarrow s \gamma) - \frac{G_F}{\sqrt{2}} V_{ts}^* V_{tb} [C_{9V}(\mu) Q_{9V} + C_{10A}(M_W) Q_{10A}] , \quad (6.3)$$

where we have again neglected the term proportional to  $V_{us}^* V_{ub}$  and  $\mathcal{H}_{\text{eff}}(b \rightarrow s \gamma)$  is given in (4.3). In addition to the operators relevant for  $B \rightarrow X_s \gamma$ , there are two new operators:

$$Q_{9V} = (\bar{s}b)_{V-A} (\bar{\mu}\mu)_V , \quad Q_{10A} = (\bar{s}b)_{V-A} (\bar{\mu}\mu)_A , \quad (6.4)$$

where  $V$  and  $A$  refer to  $\gamma_\mu$  and  $\gamma_\mu \gamma_5$ , respectively. They are generated through the electroweak penguin diagrams of fig. 1 and the related box diagrams needed mainly to keep gauge invariance.

It is convenient to work with the coefficients  $\tilde{C}_9$  and  $\tilde{C}_{10}$  defined by

$$C_{9V}(\mu) = \frac{\alpha}{2\pi} \tilde{C}_9(\mu), \quad C_{10A}(\mu) = \frac{\alpha}{2\pi} \tilde{C}_{10}(\mu). \quad (6.5)$$

Actually  $Q_{10A}$  does not renormalize under QCD and its coefficient is  $\mu$  independent with

$$\tilde{C}_{10}(\mu) = -\frac{Y(x_t, 1/R)}{\sin^2 \theta_w} \quad (6.6)$$

and  $Y(x_t, 1/R)$  defined in (3.36) and calculated in [1].

The NLO QCD corrections to  $\tilde{C}_9(\mu)$  in the SM model have been calculated in [48, 49]. Generalizing this result to the ACD model we obtain in the NDR scheme

$$\tilde{C}_9^{\text{NDR}}(\mu) = P_0^{\text{NDR}} + \frac{Y(x_t, 1/R)}{\sin^2 \theta_w} - 4Z(x_t, 1/R) + P_E E(x_t, 1/R) \quad (6.7)$$

with

$$P_0^{\text{NDR}} = 2.60 \pm 0.25 \quad (6.8)$$

as in the SM. The uncertainty comes from the  $\mu_b$  dependence, with the highest value corresponding to  $\mu_b = 2.5$  GeV and the lowest to  $\mu_b = 7.5$  GeV. The  $\mu_b$  dependence is substantially reduced through the  $\mu_b$  dependence of the perturbatively calculable matrix elements of the operators involved. Analytic formula for  $P_0^{\text{NDR}}$  can be found in [48, 49]. The functions  $Y$ ,  $Z$  and  $E$  are given in section 3.  $P_E$  is  $\mathcal{O}(10^{-2})$  and consequently the last term in (6.7) can be neglected.

In table 5 we show the  $\tilde{C}_9^{\text{NDR}}(\mu_b)$  as a function of  $1/R$  for  $m_t = 167$  GeV, different values of  $\mu_b$  and  $\alpha_s(M_Z) = 0.118$ . We observe that the impact of the KK modes on this Wilson coefficient is very small due to the approximate cancellation of these contributions to  $Y$  and  $Z$ . Consequently the impact of the KK modes on this decay proceeds almost entirely through the enhancement of the coefficient  $\tilde{C}_{10}$  and the suppression of  $C_{7\gamma}^{(0)\text{eff}}$ .

$1/R[\text{ GeV}]$	$\mu_b = 2.5 \text{ GeV}$	$\mu_b = 5.0 \text{ GeV}$	$\mu_b = 7.5 \text{ GeV}$
200	4.476	4.226	3.976
250	4.434	4.184	3.934
300	4.413	4.163	3.913
400	4.393	4.143	3.893
SM	4.372	4.122	3.872

Table 5: The values of  $\tilde{C}_9^{\text{NDR}}(\mu_b)$  in NLO for  $m_t = 167$  GeV as a function of  $1/R$  and various values of  $\mu_b$ .

### 6.3 The Differential Decay Rate

We are now ready to present the results for the differential decay rate based on the effective Hamiltonian in (6.3) and the spectator model for the matrix elements of  $Q_i$ .

Introducing

$$\hat{s} = \frac{(p_{\mu^+} + p_{\mu^-})^2}{m_b^2}, \quad z = \frac{m_c}{m_b} \quad (6.9)$$

and calculating the one-loop matrix elements of  $Q_i$  using the spectator model in the NDR scheme one finds [48, 49]

$$\tilde{T}(\hat{s}) \equiv \frac{d/d\hat{s} \Gamma(b \rightarrow s\mu^+\mu^-)}{\Gamma(b \rightarrow ce\bar{\nu})} = \frac{\alpha^2}{4\pi^2} \left| \frac{V_{ts}}{V_{cb}} \right|^2 \frac{(1-\hat{s})^2}{f(z)\kappa(z)} U(\hat{s}) \quad (6.10)$$

where

$$U(\hat{s}) = (1 + 2\hat{s}) \left( |\tilde{C}_9^{\text{eff}}(\hat{s})|^2 + |\tilde{C}_{10}|^2 \right) + 4 \left( 1 + \frac{2}{\hat{s}} \right) |C_{7\gamma}^{(0)\text{eff}}|^2 + 12C_{7\gamma}^{(0)\text{eff}} \text{Re} \tilde{C}_9^{\text{eff}}(\hat{s}) \quad (6.11)$$

and  $\tilde{C}_9^{\text{eff}}(\hat{s})$  is a function of  $\hat{s}$  that depends on the Wilson coefficient  $\tilde{C}_9^{\text{NDR}}$  and includes also contributions from four quark operators. Explicit formula can be found in [48, 49].

Next,  $f(z)$  is the phase-space factor for  $B \rightarrow X_c e \bar{\nu}$  and  $\kappa(z) = 0.88$  [50, 51] is the corresponding QCD correction. In our numerical calculations we set  $Br(B \rightarrow X_c e \bar{\nu})_{\text{exp}} = 0.104$ . Finally, the dilepton mass spectrum is defined as

$$\frac{d}{d\hat{s}} Br(B \rightarrow X_s \mu^+ \mu^-)(\hat{s}) = Br(B \rightarrow X_c e \bar{\nu})_{\text{exp}} \times \tilde{T}(\hat{s}) \equiv T(\hat{s}) . \quad (6.12)$$

Before presenting the numerical analysis let us note that among the different terms in (6.11),  $|\tilde{C}_9^{\text{eff}}(\hat{s})|^2$  is essentially as in the SM,  $|\tilde{C}_{10}|^2$  is significantly enhanced, while the last two terms in (6.11) are suppressed. However, the last term in (6.11) is negative and consequently its suppression results in an enhancement of  $U(\hat{s})$  in addition to the one due to  $\tilde{C}_{10}$ .

The formulae presented above served mainly to illustrate the pattern of various contributions that is not modified significantly at the NNLO level [24, 46, 47]. However, the latter corrections cannot be neglected and we have included them in our analysis. In obtaining these results we benefited enormously from the computer program of the authors of [44, 46] that we generalized to the ACD model.

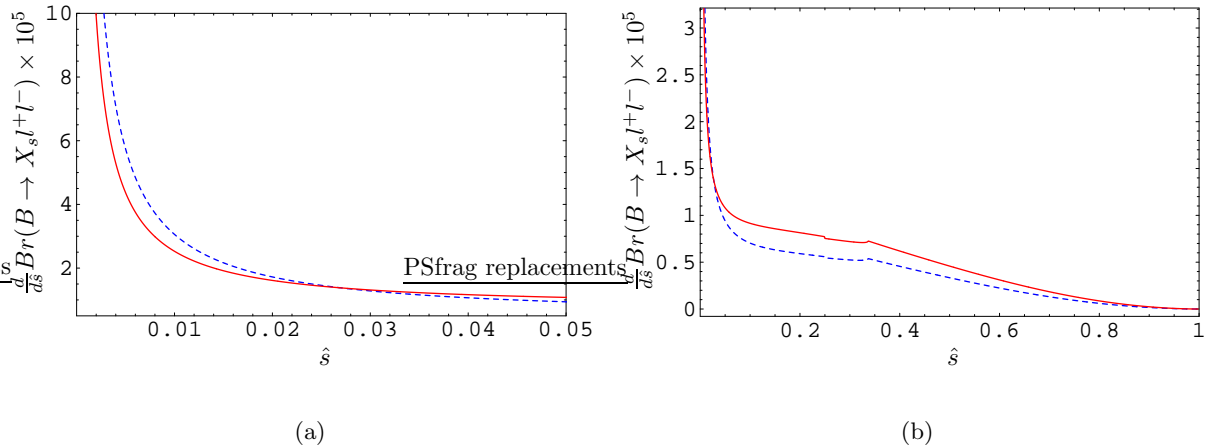


Figure 5:  $\frac{d}{d\hat{s}} Br(B \rightarrow X_s l^+ l^-)$  in the SM (dashed line) and the ACD model for  $R^{-1} = 250$  GeV. (a) Low  $\hat{s}$  region and (b) full dilepton mass spectrum.

In fig. 5 we show  $T(\hat{s})$  as a function of  $\hat{s}$  for  $1/R = 250$  GeV. As anticipated before, the KK contributions enhance  $T(\hat{s})$  with respect to the SM, see fig. 5 (b), except for very small  $\hat{s}$  where the contribution of the coefficient  $C_{7\gamma}^{(0)\text{eff}}$  dominates and its suppression results in the suppression of  $T(\hat{s})$ , see fig. 5 (a).

At this point the following remarks are in order. The theoretical calculations are cleanest for  $\hat{s}_0 \leq 0.25$  where the NNLO calculations for the inclusive decays have been completed [46, 47]

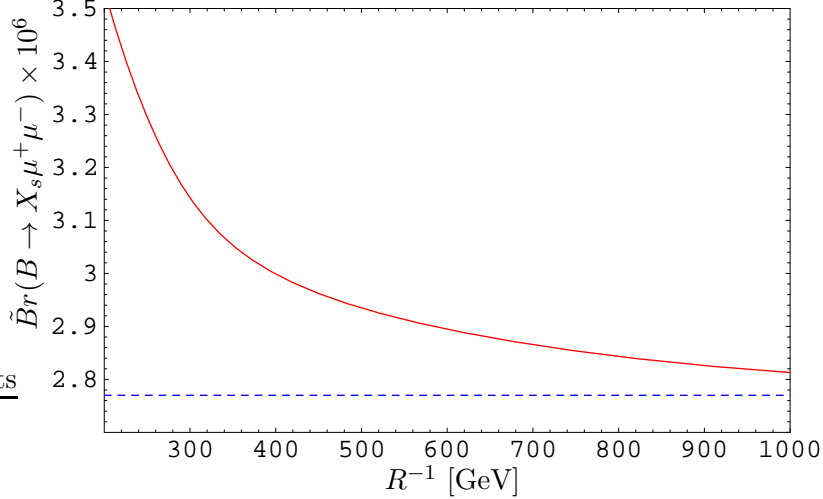


Figure 6:  $\tilde{B}r(B \rightarrow X_s \mu^+ \mu^-)$  in the SM (dashed line) and in the ACD model. The integration limits have been chosen as defined in (6.13).

and resonant effects due to  $J/\psi$ ,  $\psi'$ , etc. are expected to be small. For this reason as done in [44], we will first present the branching ratio for  $B \rightarrow X_s \mu^+ \mu^-$  by integrating over  $\hat{s}$  only in the region

$$\left(\frac{2m_\mu}{m_b}\right)^2 \leq \hat{s} \leq \left(\frac{M_{J/\psi} - 0.35 \text{ GeV}}{m_b}\right)^2 \quad (6.13)$$

that gives in the case of the SM [44] the result in (6.2) where the error comes from the variation of  $\mu_b$ ,  $m_t^{\text{pole}}$  and  $m_c/m_b$ .

In fig. 6 we show the branching ratio  $\tilde{B}r(B \rightarrow X_s \mu^+ \mu^-)$  as a function of  $1/R$ . In obtaining these results we followed closely the procedure of the authors of [44, 46] and generalized their computer programs to include the KK contributions. We observe a modest enhancement of  $\tilde{B}r(B \rightarrow X_s \mu^+ \mu^-)$  that for  $1/R = 300 \text{ GeV}$  amounts to roughly 12%.

Now the experimental number in (6.1) refers to the so-called non-resonant branching ratio integrated over the entire dilepton invariant mass spectrum. As we do not have any access to the experimental analysis and the way the resonance contributions have been removed, we will follow the authors of [44] who integrated the theoretical expressions over the whole dilepton invariant mass spectrum and obtained in the SM the result  $Br(B \rightarrow X_s \mu^+ \mu^-)_{\text{SM}} = (4.15 \pm 0.7) \cdot 10^{-6}$ . For instance for  $1/R = 300 \text{ GeV}$  we find

$$Br(B \rightarrow X_s \mu^+ \mu^-)_{\text{ACD}} = (4.8 \pm 0.8) \cdot 10^{-6}. \quad (6.14)$$

The enhancement of the relevant branching ratio is now stronger than in the previous case as the role of  $\tilde{C}_{10}$  becomes more important for larger  $\hat{s}$ . The result in (6.14) is significantly closer

to Belle's result in (6.1) than the SM prediction. However, the very large experimental error and still sizable theoretical uncertainties in the branching ratio corresponding to the full dilepton mass spectrum, also of non-perturbative origin, preclude definite conclusions at present. As we stated before it is safer to consider the branching ratio for the low dilepton mass window as given in in fig. 6.

#### 6.4 Forward-Backward Asymmetry

Of particular interest is the Forward-Backward asymmetry in  $B \rightarrow X_s \mu^+ \mu^-$ . It becomes non-zero only at the NLO level and is given in this approximation by [52]

$$A_{\text{FB}}(\hat{s}) = \frac{1}{\Gamma(b \rightarrow ce\bar{\nu})} \int_{-1}^1 d \cos \theta_l \frac{d^2 \Gamma(b \rightarrow s \mu^+ \mu^-)}{d\hat{s} d \cos \theta_l} \text{sgn}(\cos \theta_l) = -3\tilde{C}_{10} \frac{[\hat{s} \text{Re} \tilde{C}_9^{\text{eff}}(\hat{s}) + 2C_{7\gamma}^{(0)\text{eff}}]}{U(\hat{s})} \quad (6.15)$$

with  $U(\hat{s})$  given in (6.11) and where  $\theta_l$  is the angle between the  $\mu^+$  and  $B$  meson momenta in the center of mass frame. Similar to the case of exclusive decays [53], the asymmetry  $A_{\text{FB}}(\hat{s})$  vanishes at  $\hat{s} = \hat{s}_0$  that in the case of the inclusive decay considered is determined through

$$\hat{s}_0 \text{Re} \tilde{C}_9^{\text{eff}}(\hat{s}_0) + 2C_{7\gamma}^{(0)\text{eff}} = 0. \quad (6.16)$$

The fact that  $A_{\text{FB}}(\hat{s})$  and the value of  $\hat{s}_0$ , being sensitive to short distance physics, are in addition subject to only very small non-perturbative uncertainties makes them particularly useful quantities to test for physics beyond the SM.

The formulae (6.15) and (6.16) have recently been generalized to include NNLO corrections [46, 47] that turn out to be significant. In particular they shift the NLO value of  $\hat{s}_0$  from  $0.14 \pm 0.02$  to  $0.162 \pm 0.008$ . In fig. 7 (a) we show the normalized Forward-Backward asymmetry<sup>2</sup>  $\hat{A}_{\text{FB}}(\hat{s})$  for the central values of the input parameters that we obtained by means of the formulae and the computer program of [44, 46] modified by the KK contributions calculated here. The dependence of  $\hat{s}_0$  on  $1/R$  is shown in fig. 7 (b).

We observe that the value of  $\hat{s}_0$  is considerably reduced relative to the SM result obtained including NNLO corrections [44, 46, 47]. This decrease originates in the suppression of the coefficient  $C_{7\gamma}^{(0)\text{eff}}$  as clearly seen in (6.16). We recall that  $\tilde{C}_9^{\text{eff}}$  is only weakly affected by the KK contributions. For  $1/R = 300 \text{ GeV}$  we find a value for  $\hat{s}_0$  that is very close to the NLO prediction of the SM. This result demonstrates very clearly the importance of the higher order QCD corrections, in particular in quantities like  $\hat{s}_0$  that are theoretically clean. We expect that the results in figs. 7 (a) and (b) will play an important role in the tests of the ACD model in the future.

---

<sup>2</sup>The normalized FB asymmetry is given as  $\hat{A}_{\text{FB}}(\hat{s}) = \Gamma(b \rightarrow ce\bar{\nu}) \times A_{\text{FB}}(\hat{s}) / \int_{-1}^1 d \cos \theta_l \frac{d^2 \Gamma(b \rightarrow s \mu^+ \mu^-)}{d\hat{s} d \cos \theta_l}$

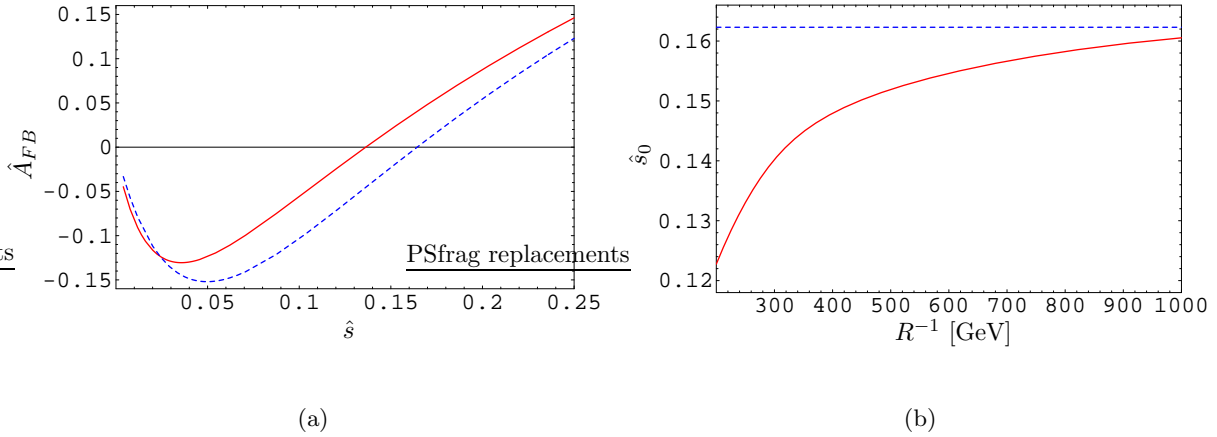


Figure 7: (a) Normalized Forward-Backward asymmetry in the SM (dashed line) and ACD for  $R^{-1} = 250$  GeV. (b) Zero of the forward backward asymmetry  $A_{FB}$  in the SM (dashed line) and the ACD model.

### 6.5 Correlation between $\hat{s}_0$ and $Br(B \rightarrow X_s \gamma)$

In MFV models there exist a number of correlations between different measurable quantities that do not depend on specific parameters of a given model. These correlations originate in the general property of these models: the new physics enters only through the Inami-Lim (IL) functions. As several processes depend on the same IL functions, eliminating these functions in favour of measurable quantities allows to derive interesting universal relations between these quantities that do not involve parameters specific to a given model. Examples can be found in [17, 54].

Here we would like to point out a correlation between  $\hat{s}_0$  and  $Br(B \rightarrow X_s \gamma)$  that is present in the ACD model and in any MFV model in which new physics contributions to  $\tilde{C}_9^{\text{eff}}$  and its  $\hat{s}$  dependence can be neglected to first approximation. This is the case of the ACD model and of a large class of supersymmetric models discussed for instance in [44]. As new physics contributions to the  $Z^0$ -penguin represented by the function  $C$  are suppressed in  $\tilde{C}_9^{\text{eff}}$  by the factor  $(4 \sin^2 \theta_w - 1)$ , the necessary requirement for the weak dependence of  $\tilde{C}_9^{\text{eff}}$  on new physics is the smallness of these contributions to the  $B$  and  $D$  functions. This in fact is the case for many MFV models.

If  $\tilde{C}_9^{\text{eff}}$  is unaffected by new physics contributions and its  $\hat{s}$ -dependence is weak then, as seen in (6.16),  $\hat{s}_0$  is simply proportional to  $C_{7\gamma}^{(0)\text{eff}}$  with the proportionality factor independent of new physics. Consequently  $\hat{s}_0$  is proportional to  $\sqrt{Br(B \rightarrow X_s \gamma)}$ ,

$$\hat{s}_0 \propto \frac{\sqrt{Br(B \rightarrow X_s \gamma)}}{\tilde{C}_9^{\text{eff}}}, \quad (6.17)$$

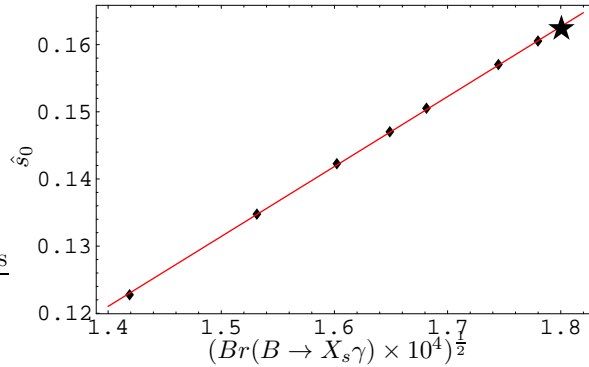


Figure 8: Correlation between  $\sqrt{Br(B \rightarrow X_s \gamma)}$  and  $\hat{s}_0$ . The straight line is a least square fit to a linear function. The dots are the results in the ACD model for  $1/R = 200, 250, 300, 350, 400, 600$  and  $1000$  GeV and the star denotes the SM value.

and can simply be predicted from the measured value of  $Br(B \rightarrow X_s \gamma)$  and  $\tilde{C}_9^{\text{eff}}$  given in the SM. This correlation is shown in fig. 8. It depends of course on the relation between  $C_{7\gamma}^{(0)\text{eff}}$  and  $Br(B \rightarrow X_s \gamma)$ , in particular on  $m_c/m_b$ . In fig. 8 we have used  $m_c/m_b = 0.29$ . The plot in fig. 8 has been obtained within the ACD model by expressing  $1/R$  in fig. 7 (b) through  $Br(B \rightarrow X_s \gamma)$  by means of the results in fig. 3. The fact that the result of this exercise is a straight line confirms our result that the new physics contributions to  $\tilde{C}_9^{\text{eff}}$  and its  $\hat{s}$  dependence are small.

## 7 $K_L \rightarrow \pi^0 e^+ e^-$

### 7.1 Preliminaries

There are three contributions to this decay: CP-conserving, indirectly CP-violating and directly CP-violating. Unfortunately out of these three contributions only the directly CP-violating one can be calculated reliably. In this contribution there are practically no theoretical uncertainties related to hadronic matrix elements because  $\langle \pi^0 | (\bar{s}d)_{V-A} | K_L \rangle$  can be extracted using isospin symmetry from the well measured decay  $K^+ \rightarrow \pi^0 e^+ \nu$ . In what follows we will only consider this contribution. Most recent reviews of  $K_L \rightarrow \pi^0 e^+ e^-$  with references to earlier literature can be found in [55].

### 7.2 The Branching Ratio

Generalizing the NLO formula in [56] to the ACD model we obtain

$$Br(K_L \rightarrow \pi^0 e^+ e^-)_{\text{dir}} = \kappa_e (\text{Im} \lambda_t)^2 (\tilde{y}_{7A}^2 + \tilde{y}_{7V}^2), \quad (7.18)$$

where  $\text{Im}\lambda_t = \text{Im}(V_{td}V_{ts}^*)$ ,

$$\kappa_e = \frac{1}{V_{us}^2} \frac{\tau(K_L)}{\tau(K^+)} \left(\frac{\alpha}{2\pi}\right)^2 Br(K^+ \rightarrow \pi^0 e^+ \nu) = 6.34 \cdot 10^{-6} \quad (7.19)$$

and

$$\tilde{y}_{7V} = P_0 + \frac{Y(x_t, 1/R)}{\sin^2 \theta_w} - 4Z(x_t, 1/R) + P_E E(x_t, 1/R) , \quad (7.20)$$

$$\tilde{y}_{7A} = -\frac{1}{\sin^2 \theta_w} Y(x_t, 1/R) \quad (7.21)$$

with  $Y(x_t, 1/R)$ ,  $Z(x_t, 1/R)$  and  $E(x_t, 1/R)$  given in section 3. The formula (7.20) has a structure identical to (6.7) relevant for  $B \rightarrow X_s \mu^+ \mu^-$  with different numerical values for  $P_0$  and  $P_E$  due to different scales  $\mu$  involved.  $P_E$  is  $\mathcal{O}(10^{-2})$  and consequently the last term in (7.20) can be neglected. The next-to-leading QCD corrections to the coefficients above enter only  $P_0$ . They have been calculated in [56]. One finds  $P_0 = 3.05 \pm 0.06$ , where the error comes from the  $\alpha_s$  and scale uncertainties. Similarly to  $B \rightarrow X_s \mu^+ \mu^-$ , the effect of KK contributions is mainly felt in  $\tilde{y}_{7A}$ .

The present experimental bound from KTeV [57]

$$Br(K_L \rightarrow \pi^0 e^+ e^-) < 3.5 \cdot 10^{-10} \quad (90\%C.L.) \quad (7.22)$$

is still by two orders of magnitude away from the theoretical expectations in the SM and the ACD model.

### 7.3 Numerical Analysis

In table 6 we show  $Br(K_L \rightarrow \pi^0 e^+ e^-)_{\text{dir}}$  in the ACD model as a function of  $1/R$  for  $P_0 = 3.05$  and  $m_t = 167 \text{ GeV}$ . We also show there  $\text{Im}\lambda_t$ . To this end we have used the analysis of the unitarity triangle of [1]. The enhancement of  $Br(K_L \rightarrow \pi^0 e^+ e^-)_{\text{dir}}$  is at most 10% because the enhancement of the function  $Y$  in  $\tilde{y}_{7A}$  is compensated to a large extent by the suppression of  $\text{Im}\lambda_t$ .

$1/R$ [GeV]	200	250	300	400	SM
$\text{Im}\lambda_t \times 10^4$	1.202	1.250	1.276	1.302	1.333
$Br(K_L \rightarrow \pi^0 e^+ e^-)_{\text{dir}} \times 10^{12}$	4.87	4.77	4.69	4.58	4.39

Table 6: Values for  $\text{Im}\lambda_t$  and  $Br(K_L \rightarrow \pi^0 e^+ e^-)_{\text{dir}}$  for different  $1/R$ .

## 8 The Ratio $\varepsilon'/\varepsilon$

### 8.1 Preliminaries

The ratio  $\varepsilon'/\varepsilon$  that parametrizes the size of the direct CP violation with respect to the indirect CP violation in  $K_L \rightarrow \pi\pi$  decays has been the subject of very intensive experimental and theoretical studies. On the experimental side the world average based on the recent results from NA48 [58] and KTeV [59] and previous results from NA31 and E731 collaborations reads

$$\varepsilon'/\varepsilon = (16.6 \pm 1.6) \cdot 10^{-4} . \quad (8.1)$$

On the other hand, the theoretical estimates of this ratio are subject to very large hadronic uncertainties. While several analyses within the SM find results that are compatible with (8.1), it is fair to say that the chapter on the theoretical calculations of  $\varepsilon'/\varepsilon$  is certainly open. Most recent reviews with references to original papers can be found in [60, 61, 62].

In view of this situation, our strategy will be to choose various sets of the values of the main non-perturbative parameters  $B_6^{(1/2)}$  and  $B_8^{(3/2)}$  for a fixed strange quark mass  $m_s(m_c)$  and to investigate for each chosen set  $(B_6^{(1/2)}, B_8^{(3/2)})$  the impact of the KK modes on  $\varepsilon'/\varepsilon$ .

### 8.2 Basic Formula

The formula for  $\varepsilon'/\varepsilon$  of [63, 64] generalizes to the ACD model as follows:

$$\frac{\varepsilon'}{\varepsilon} = \text{Im}\lambda_t \cdot F_{\varepsilon'}(x_t, 1/R) , \quad (8.2)$$

where

$$F_{\varepsilon'}(x_t, 1/R) = P_0 + P_X X(x_t, 1/R) + P_Y Y(x_t, 1/R) + P_Z Z(x_t, 1/R) + P_E E(x_t, 1/R) \quad (8.3)$$

with the functions  $X$ ,  $Y$ ,  $Z$ ,  $E$  given in section 3. Strictly speaking the functions  $X$  and  $Y$  entering (8.3) are given by  $X = C + B^{(uu)}$  and  $Y = C + B^{(dd)}$  and consequently they differ slightly from the ones defined in (3.35) and (3.36) that involve  $B^{\nu\bar{\nu}}$  and  $B^{\mu\bar{\mu}}$  instead of  $B^{(uu)}$  and  $B^{(dd)}$ , respectively. However, this difference caused only by the KK contributions to the box diagrams is fully negligible and the numerical values for  $X$  and  $Y$  given in table 1 can also be used here.

The coefficients  $P_i$  are given in terms of the non-perturbative parameters  $B_6^{(1/2)}$  and  $B_8^{(3/2)}$  and the strange quark mass  $m_s(m_c)$  as follows:

$$P_i = r_i^{(0)} + r_i^{(6)} R_6 + r_i^{(8)} R_8 , \quad (8.4)$$

where

$$R_6 \equiv B_6^{(1/2)} \left[ \frac{121 \text{ MeV}}{m_s(m_c) + m_d(m_c)} \right]^2, \quad R_8 \equiv B_8^{(3/2)} \left[ \frac{121 \text{ MeV}}{m_s(m_c) + m_d(m_c)} \right]^2. \quad (8.5)$$

$B_6^{(1/2)}$  and  $B_8^{(3/2)}$  parameterize the matrix elements of the dominant QCD-penguin ( $Q_6$ ) and the dominant electroweak penguin ( $Q_8$ ) operator, respectively. The numerical values of  $r_i^{(0)}$ ,  $r_i^{(6)}$  and  $r_i^{(8)}$  for different values of  $\Lambda_{\overline{\text{MS}}}^{(4)}$  at  $\mu = m_c$  have recently been updated in [62] and are given in the NDR renormalization scheme in table 7.

	$\Lambda_{\overline{\text{MS}}}^{(4)} = 310 \text{ MeV}$			$\Lambda_{\overline{\text{MS}}}^{(4)} = 340 \text{ MeV}$			$\Lambda_{\overline{\text{MS}}}^{(4)} = 370 \text{ MeV}$		
$i$	$r_i^{(0)}$	$r_i^{(6)}$	$r_i^{(8)}$	$r_i^{(0)}$	$r_i^{(6)}$	$r_i^{(8)}$	$r_i^{(0)}$	$r_i^{(6)}$	$r_i^{(8)}$
0	-3.167	14.781	1.815	-3.192	15.974	1.686	-3.215	17.277	1.546
X	0.546	0.026	0	0.537	0.029	0	0.529	0.032	0
Y	0.395	0.107	0	0.385	0.113	0	0.376	0.120	0
Z	0.626	-0.020	-12.574	0.673	-0.021	-13.226	0.723	-0.023	-13.927
E	0.189	-1.705	0.552	0.179	-1.801	0.592	0.169	-1.903	0.634

Table 7: Coefficients in the formula (8.4) for various  $\Lambda_{\overline{\text{MS}}}^{(4)}$  in the NDR scheme [62].

### 8.3 Numerical Analysis

The values of  $\text{Im}\lambda_t$  for various values of  $1/R$  are given in table 6. In table 8 we show the corresponding results for  $\varepsilon'/\varepsilon$  as functions of the non-perturbative parameters in question. To this end we have set  $m_s(m_c) = 100 \text{ MeV}$  which corresponds to  $m_s(2 \text{ GeV}) = 85 \text{ MeV}$ , in the ballpark of some most recent lattice calculations with dynamical fermions [65]. The last year lattice values [66] and the QCD sum rules values [67] are slightly higher:  $m_s(m_c) = 115 \pm 20 \text{ MeV}$ .

The results in table 8 are self explanatory. Dependently on the values of the parameters  $B_6^{(1/2)}$  and  $B_8^{(3/2)}$  one finds the value of  $1/R$  that is favoured by the experimental data. Only for the case  $(B_6^{(1/2)}, B_8^{(3/2)}) = (1.0, 1.0)$  the results for  $\varepsilon'/\varepsilon$  are outside the experimental range in (8.1) independently of  $1/R$  considered. As for  $310 \text{ MeV} \leq \Lambda_{\overline{\text{MS}}}^{(4)} \leq 370 \text{ MeV}$  the ratio  $\varepsilon'/\varepsilon$  is approximately proportional to  $\Lambda_{\overline{\text{MS}}}^{(4)}$ , the results in table 8 can be at most changed by  $\pm 10\%$ .

Clearly, the hadronic uncertainties in  $(B_6^{(1/2)}, B_8^{(3/2)})$  and  $m_s(m_c)$  preclude any determination of  $1/R$  from the data on  $\varepsilon'/\varepsilon$  at present. As generally  $\varepsilon'/\varepsilon$  is suppressed by the KK mode contributions relatively to the SM, the ACD model is disfavoured by  $\varepsilon'/\varepsilon$  unless  $(B_6^{(1/2)}, B_8^{(3/2)})$  and  $m_s(m_c)$  or generally the matrix elements of  $Q_6$  and  $Q_8$  are such that the SM estimates are above the data. This is the case for sufficiently low values of  $m_s(m_c)$  and sufficiently high values

	$B_6^{(1/2)} = 1.00$		$B_6^{(1/2)} = 1.15$		$B_6^{(1/2)} = 1.30$	
$1/R$	$B_8^{(3/2)} = 0.8$	$B_8^{(3/2)} = 1.0$	$B_8^{(3/2)} = 0.8$	$B_8^{(3/2)} = 1.0$	$B_8^{(3/2)} = 0.8$	$B_8^{(3/2)} = 1.0$
200	9.1	5.6	12.7	9.2	16.4	12.9
250	11.0	7.7	14.8	11.5	18.6	15.3
300	12.1	9.1	16.0	12.9	19.9	16.8
400	13.4	10.6	17.3	14.5	21.3	18.5
SM	15.2	12.8	19.3	16.8	23.4	20.9

Table 8: The ratio  $\varepsilon'/\varepsilon$  in units of  $10^{-4}$  for  $m_t = 167$  GeV,  $\Lambda_{\overline{\text{MS}}}^{(4)} = 340$  MeV,  $m_s(m_c) = 100$  MeV and  $m_d(m_c) = 6$  MeV as a function of  $1/R$  in GeV and various values of  $B_6^{(1/2)}$  and  $B_8^{(3/2)}$ .

of  $B_6^{(1/2)}$ . For these cases a suppression of  $\varepsilon'/\varepsilon$  by the KK modes found here is a welcome feature of the ACD model.

## 9 Summary and Outlook

In this paper we have calculated for the first time the contributions of the Kaluza-Klein (KK) modes to  $B \rightarrow X_s$  gluon,  $B \rightarrow X_s \mu^+ \mu^-$  and  $K_L \rightarrow \pi^0 e^+ e^-$  and to the CP-violating ratio  $\varepsilon'/\varepsilon$  in the Appelquist, Cheng and Dobrescu (ACD) model with one universal extra dimension. We have also analyzed  $B \rightarrow X_s \gamma$  that has been considered in the past [3]. While our result for this decay differs in details from the latter paper, we confirm the suppression of the relevant branching ratio found by these authors. As a byproduct we have given a list of the required Feynman rules involving photons and gluons that have not been presented in the literature so far. Moreover we have generalized the background field method to five dimensions.

The nice property of this extension of the SM is the presence of only a single new parameter,  $1/R$ . This economy in new parameters should be contrasted with supersymmetric theories and models with an extended Higgs sector. Taking  $1/R = 300$  GeV our findings are as follows:

- The short distance function  $Z$ , relevant for  $B \rightarrow X_s \mu^+ \mu^-$ ,  $K_L \rightarrow \pi^0 e^+ e^-$  and  $\varepsilon'/\varepsilon$  is enhanced by 23% relative to the SM value.
- The functions  $D'$  and  $E'$ , relevant for  $B \rightarrow X_s \gamma$  and  $B \rightarrow X_s$  gluon are suppressed by 36% and 66%, respectively. The corresponding effects in the function  $D$  are negligible and in  $E$  phenomenologically irrelevant.
- $Br(B \rightarrow X_s \gamma)$  is suppressed by 20%. The phenomenological implications of this result depend sensitively on the value of  $m_c/m_b$  and on the experimental data, with the lower

bound on  $1/R$  being stronger for  $m_c/m_b=0.29$  than for  $m_c/m_b=0.22$ . In fact, in the latter case the suppression of  $Br(B \rightarrow X_s\gamma)$  could be welcome and an upper bound on  $1/R$  could in principle be found when the experimental and theoretical uncertainties decrease.

- $Br(B \rightarrow X_s \text{ gluon})$  is suppressed by 40%. The phenomenological relevance of this result is, in view of large hadronic uncertainties and the difficulty in extracting this branching ratio from the data, unclear at present.
- The perturbative part of  $Br(B \rightarrow X_s\mu^+\mu^-)$  is enhanced by 12%. This could be a welcome feature of the ACD model in view of the data from Belle, that is above the SM expectations. However, more interesting is the shift of the zero in the  $A_{FB}$  asymmetry from  $\hat{s}_0 = 0.162$  to  $\hat{s}_0 = 0.142$ , that in view of small theoretical uncertainties could turn out to be a very important test of the ACD model.
- We have pointed out a correlation between the zero  $\hat{s}_0$  in the  $A_{FB}$  asymmetry and  $Br(B \rightarrow X_s\gamma)$  that should be valid in most models with minimal flavour violation. This correlation is shown in fig. 8.
- $Br(K_L \rightarrow \pi^0 e^+ e^-)$  is enhanced by less than 10%.
- $\varepsilon'/\varepsilon$  is suppressed relative to the SM expectations with the size of the suppression depending sensitively on the hadronic matrix elements. Taking  $m_s(2 \text{ GeV}) = 85 \text{ MeV}$  as suggested by the most recent lattice calculations, we find that for several sets of  $(B_6^{(1/2)}, B_8^{(3/2)})$  the ACD model can be made compatible with the experimental data, see table 8 for details.

These findings should be compared with the ones of [1], where for  $1/R = 300 \text{ GeV}$  the following enhancements relative to the SM predictions due to enhanced  $Z^0$ -penguins have been found:  $K^+ \rightarrow \pi^+\nu\bar{\nu}$  (9%),  $K_L \rightarrow \pi^0\nu\bar{\nu}$  (10%),  $B \rightarrow X_d\nu\bar{\nu}$  (12%),  $B \rightarrow X_s\nu\bar{\nu}$  (21%),  $K_L \rightarrow \mu\bar{\mu}$  (20%),  $B_d \rightarrow \mu\bar{\mu}$  (23%) and  $B_s \rightarrow \mu\bar{\mu}$  (33%).

We observe that the impact of the KK modes on  $B \rightarrow X_s\gamma$  is comparable to the one on  $B \rightarrow X_s\nu\bar{\nu}$ ,  $K_L \rightarrow \mu\bar{\mu}$  and  $B_d \rightarrow \mu\bar{\mu}$ . The corresponding impact on  $B \rightarrow X_s \text{ gluon}$  is significantly larger and comparable to the one on  $B_s \rightarrow \mu^+\mu^-$ . On the whole, the main effects of the KK modes are felt in  $Z^0$ -penguins,  $\gamma$ -magnetic penguins and chromomagnetic penguins.

Moreover, the low compactification scale  $200 \text{ GeV}$  that was fully compatible with the data on the decays considered there, is excluded by the  $B \rightarrow X_s\gamma$  decay. For  $1/R = 200 \text{ GeV}$  the branching ratio  $Br(B \rightarrow X_s\gamma)$  is suppressed relative to the SM by a factor of 1.6. This is clearly excluded. Of considerable interest is an even stronger suppression of  $B \rightarrow X_s \text{ gluon}$ .

Interestingly, the present data on  $K^+ \rightarrow \pi^+\nu\bar{\nu}$  and  $B \rightarrow X_s\mu^+\mu^-$  are somewhat above the SM expectations and the *enhancement* of the  $Z^0$ -penguins by the KK modes could be welcome

in this context. On the other hand, the present central experimental values for  $Br(B \rightarrow X_s \gamma)$  are somewhat below the SM expectations and the *suppression* of the magnetic penguins by the KK modes could also be welcome. However, in all these cases the experimental and theoretical uncertainties have to be reduced in order to be definitive about the need for these enhancements and suppressions.

Whether the suppression of  $B \rightarrow X_s$  gluon and of  $\varepsilon'/\varepsilon$  by the KK modes relative to the SM expectations is a welcome feature depends very strongly on hadronic uncertainties and in the case of  $B \rightarrow X_s$  gluon on the data.

Possibly, the most interesting result of our paper is the sizable downward shift of the zero ( $\hat{s}_0$ ) in the  $A_{FB}$  asymmetry. It should be emphasized that this shift has a definite sign and the theoretical uncertainties in its value are small.

Our present analysis combined with our previous paper [1] completes the study of the most interesting FCNC processes in the ACD model. With only one additional parameter, the compactification scale, the pattern of various enhancements and suppressions relative to the SM expectations could be uniquely determined:

- Enhancements:  $K_L \rightarrow \pi^0 e^+ e^-$ ,  $\Delta M_s$ ,  $K^+ \rightarrow \pi^+ \nu \bar{\nu}$ ,  $K_L \rightarrow \pi^0 \nu \bar{\nu}$ ,  $B \rightarrow X_d \nu \bar{\nu}$ ,  $B \rightarrow X_s \nu \bar{\nu}$ ,  $K_L \rightarrow \mu^+ \mu^-$ ,  $B_d \rightarrow \mu^+ \mu^-$ ,  $B \rightarrow X_s \mu^+ \mu^-$  and  $B_s \rightarrow \mu^+ \mu^-$ .
- Suppressions:  $B \rightarrow X_s \gamma$ ,  $B \rightarrow X_s$  gluon, the value of  $\hat{s}_0$  in the forward-backward asymmetry and  $\varepsilon'/\varepsilon$ .

Whether these enhancements and suppressions are required by the data or whether they exclude the ACD model with a low compactification scale, will depend on the precision of the forthcoming experiments and the efforts to decrease the theoretical uncertainties.

## Acknowledgements

We would like to thank first of all Christoph Greub but also Christoph Bobeth, Paolo Gambino, Uli Haisch, Gudrun Hiller, Matthias Jamin, Mikolaj Misiak and Jörg Urban for discussions related to their work within the SM on the decays considered in this paper and for providing the relevant NLO and NNLO computer programs that accelerated considerably our work. We also thank Gino Isidori and Frank Krüger for informative discussions on the  $B \rightarrow X_s \mu^+ \mu^-$  decay. This research was partially supported by the German ‘Bundesministerium für Bildung und Forschung’ under contract 05HT1WOA3 and by the ‘Deutsche Forschungsgemeinschaft’ (DFG) under contract Bu.706/1-2.

## A Background Field method in 5 dimensions

In the calculation of the off-shell amplitude, we have used the method of background fields. As in 1-PI diagrams the background fields only appear on the external legs, there is no need to fix the gauge for the background gauge fields. With the appropriate choice of the gauge fixing for the quantum gauge fields, we can ensure the invariance of the effective action with respect to background field (BF) gauge transformations. The general procedure in 4 dimensions is described in [25]. Here we only state the SM case and modify the gauge fixing to fit the ACD model.

The starting point is the action  $S[\psi]$  before gauge fixing, where  $\psi$  denotes all gauge and matter fields in the action. We get the BF action by the transformation

$$S[\psi] \longrightarrow S[\psi + \hat{\psi}], \quad (\text{A.1})$$

where we have introduced the background fields  $\hat{\psi}$ . It is modified by the gauge fixing to

$$S_{\text{BF}}[\psi, \hat{\psi}] = S[\psi + \hat{\psi}] - \frac{1}{2\xi} \int d^d x \tilde{\mathcal{G}}\tilde{\mathcal{G}} + \text{ghost terms}, \quad (\text{A.2})$$

where  $\tilde{\mathcal{G}}\tilde{\mathcal{G}}$  stands for all gauge fixing functionals. As the terms with ghost fields are not relevant for us we will not consider them here.

In the 4-dimensional electroweak SM, a convenient choice for the gauge fixing functionals is

$$\tilde{\mathcal{G}}_{B,\text{SM}}[B, \phi, \hat{\phi}] = \partial_\mu B^\mu - ig'\xi \frac{1}{2} (\hat{\phi}^\dagger \phi - \phi^\dagger \hat{\phi}), \quad (\text{A.3})$$

$$\tilde{\mathcal{G}}_{A,\text{SM}}^a[A, \hat{A}, \phi, \hat{\phi}] = \partial_\mu A^{a\mu} + g_2 \epsilon^{abc} \hat{A}_\mu^b A^{c\mu} - ig_2 \xi \frac{1}{2} (\hat{\phi}^\dagger \sigma^a \phi - \phi^\dagger \sigma^a \hat{\phi}), \quad (\text{A.4})$$

with the Higgs fields

$$\hat{\phi} = \frac{1}{\sqrt{2}} (v + \hat{\psi} + i\hat{\chi}^a \sigma^a) \begin{pmatrix} 0 \\ 1 \end{pmatrix}, \quad \phi = \frac{1}{\sqrt{2}} (\psi + i\chi^a \sigma^a) \begin{pmatrix} 0 \\ 1 \end{pmatrix}, \quad (\text{A.5})$$

where  $\sigma^a$  are the common Pauli matrices. According to (A.2), the gauge fixing part of the Lagrangian is

$$\mathcal{L}_{\text{GF}} = -\frac{1}{2\xi} \tilde{\mathcal{G}}_B \tilde{\mathcal{G}}_B - \frac{1}{2\xi} \tilde{\mathcal{G}}_A^a \tilde{\mathcal{G}}_A^a. \quad (\text{A.6})$$

With this specific gauge fixing, the BF action is invariant under the BF gauge transformation<sup>3</sup>

$$\delta_{\text{BF}} \hat{B}_\mu = \frac{1}{g'} \partial_\mu \beta, \quad (\text{A.7})$$

$$\delta_{\text{BF}} \hat{A}_\mu^a = f^{abc} \hat{A}_\mu^b \alpha^c + \frac{1}{g_2} \partial_\mu \alpha^a, \quad (\text{A.8})$$

$$\delta_{\text{BF}} \hat{\phi} = i \left( \alpha^a \frac{\sigma^a}{2} + \frac{1}{2} \beta \right) \hat{\phi}, \quad (\text{A.9})$$

---

<sup>3</sup>We omit the BF gauge transformation of the fermions which is just an ordinary gauge transformation.

combined with a transformation of the quantum fields

$$\delta A_\mu^a = f^{abc} A_\mu^b \alpha^c, \quad (\text{A.10})$$

$$\delta \phi = i \left( \alpha^a \frac{\sigma^a}{2} + \frac{1}{2} \beta \right) \phi, \quad (\text{A.11})$$

where (A.10) and (A.11) are just unitary rotations in the functional integral.

The analogous BF gauge transformation in 5 dimensions is

$$\delta_{\text{BF}} \hat{B}_M = \frac{1}{\hat{g}'} \partial_M \beta, \quad (\text{A.12})$$

$$\delta_{\text{BF}} \hat{A}_M^a = f^{abc} \hat{A}_M^b \alpha^c + \frac{1}{\hat{g}_2} \partial_M \alpha^a, \quad (\text{A.13})$$

$$\delta_{\text{BF}} \hat{\phi} = i \left( \alpha^a \frac{\sigma^a}{2} + \frac{1}{2} \beta \right) \hat{\phi} \quad (\text{A.14})$$

combined with

$$\delta A_M^a = f^{abc} A_M^b \alpha^c, \quad (\text{A.15})$$

$$\delta \phi = i \left( \alpha^a \frac{\sigma^a}{2} + \frac{1}{2} \beta \right) \phi. \quad (\text{A.16})$$

Compared to 4 dimensions, the couplings  $g'$  and  $g_2$  have been replaced by their 5-dimensional analogs  $\hat{g}'$  and  $\hat{g}_2$ . All fields and  $\alpha^a$  and  $\beta$  are now also functions of the extra coordinate  $y$  and the vector index  $M$  can take the values  $M = 0, 1, 2, 3, 5$ .

In the ACD model, we have to add  $-\xi \partial_5 B_5$  to (A.3) and  $-\xi \partial_5 A_5^a$  to (A.4) in order to diagonalize the mass matrices of the bosonic modes [1]. However, this spoils BF gauge invariance, so we add another term to (A.4) to fix this and get

$$\tilde{\mathcal{G}}_{B,\text{ACD}}[B, \phi, \hat{\phi}] = \tilde{\mathcal{G}}_{B,\text{SM}}[B, \phi, \hat{\phi}] - \xi \partial_5 B_5, \quad (\text{A.17})$$

$$\tilde{\mathcal{G}}_{A,\text{ACD}}^a[A, \hat{A}, \phi, \hat{\phi}] = \tilde{\mathcal{G}}_{A,\text{SM}}^a[A, \hat{A}, \phi, \hat{\phi}] - \xi \partial_5 A_5^a - \xi \hat{g}_2 \epsilon^{abc} \hat{A}_5^b A_5^c, \quad (\text{A.18})$$

where it is understood that  $g'$  and  $g_2$  have been replaced by  $\hat{g}'$  and  $\hat{g}_2$ .

The use of (A.17) and (A.18) ensures invariance of all 1-PI diagrams under BF gauge transformations in 5 dimensions. However, as we are only interested in external zero-mode fields, the last term in (A.18) does not affect our calculation.

In the diagrams for the calculation of the functions  $E$  and  $E'$ , the external gluon couples only to the quarks. As there are no fermions involved in the gauge fixing, the background gluon couples to quarks just like a quantum gluon, and there is no need to specify a gauge fixing functional for QCD. For completeness, we note that

$$\tilde{\mathcal{G}}_{G,\text{ACD}}^a[G, \hat{G}] = \partial_\mu G^{a\mu} + \hat{g}_s f^{abc} \hat{G}_\mu^b G^{c\mu} - \xi \partial_5 G_5^a - \xi \hat{g}_s f^{abc} \hat{G}_5^b G_5^c \quad (\text{A.19})$$

would be an appropriate choice. Here  $f^{abc}$  are the  $SU(3)_C$  structure constants and  $\hat{g}_s$  is the strong coupling constant.

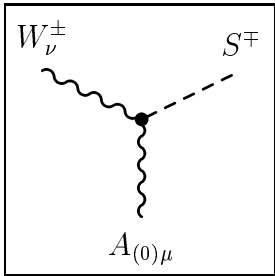
## B Feynman Rules in the ACD Model: Photon and Gluons

In this section we list the Feynman rules needed for the calculations in this paper except for those already given in [1]. The Feynman rules are derived in the 5d background field  $R_\xi$ -gauge described in appendix A. The rules for vertices involving only quantum fields are the same as in the conventional 5d  $R_\xi$ -gauge described in [1].

In order to simplify the notation, we omit the KK indices of the fields. There is no ambiguity because in one-loop calculations at least one field is always a zero-mode. In the vertex rules given below, this is the photon  $A$ , the gluon  $G$  and their background equivalents. Due to KK parity conservation, the other two fields have equal KK mode number, i.e. either zero or  $n \geq 1$ .

Fermion zero-modes have substantially different Feynman rules than their KK excitations. The up-type quarks  $\mathcal{Q}_i$  and  $\mathcal{U}_i$  are always supposed to be  $(n \geq 1)$ -modes, while the zero-mode is labeled  $u$ . The generation index  $i$  can take the values  $i = u, c, t$ .

In the vertices below,  $S^\pm$  stands for the scalar modes  $G^\pm$  and  $a^\pm$ . All momenta and fields are assumed to be incoming. The Feynman rules for the vertices are:



$$= g_2 s_w M_{W(n)} g_{\mu\nu} C.$$

$$AW^+G^- : C = 1, \quad AW^-G^+ : C = -1, \quad (\text{B.1})$$

$$AW^+a^- : C = 0, \quad AW^-a^+ : C = 0, \quad (\text{B.2})$$

$$\hat{A}W^+G^- : C = 0, \quad \hat{A}W^-G^+ : C = 0, \quad (\text{B.3})$$

$$\hat{A}W^+a^- : C = 0, \quad \hat{A}W^-a^+ : C = 0. \quad (\text{B.4})$$

$$= -ig_2s_w(k_2 - k_1)_\mu C.$$

$$AG^+G^- : C = 1, \quad Aa^+a^- : C = 1, \quad (\text{B.5})$$

$$AG^+a^- : C = 0, \quad Aa^+G^- : C = 0, \quad (\text{B.6})$$

and the same values of  $C$  for the analogous vertices with a background photon  $\hat{A}$ .

$$= ig_2s_w C.$$

$$AW^+W^- : C = g_{\mu\nu}(k_2 - k_1)_\lambda + g_{\mu\lambda}(k_1 - k_3)_\nu + g_{\lambda\nu}(k_3 - k_2)_\mu, \quad (\text{B.7})$$

$$\hat{A}W^+W^- : C = g_{\mu\nu}(k_2 - k_1 + \frac{1}{\xi}k_3)_\lambda + g_{\mu\lambda}(k_1 - k_3 - \frac{1}{\xi}k_2)_\nu \quad (\text{B.8})$$

$$+ g_{\lambda\nu}(k_3 - k_2)_\mu. \quad (\text{B.9})$$

$$= ig_2s_w\gamma_\mu C.$$

$$A\bar{u}_i u_i : C = \frac{2}{3}, \quad (\text{B.10})$$

$$A\bar{Q}_i Q_i : C = \frac{2}{3}, \quad A\bar{U}_i U_i : C = \frac{2}{3}, \quad (\text{B.11})$$

$$A\bar{Q}_i U_i : C = 0, \quad A\bar{U}_i Q_i : C = 0, \quad (\text{B.12})$$

and the same values of  $C$  for the analogous vertices with a background photon  $\hat{A}$ .

A Feynman diagram enclosed in a square box. It shows a central black dot representing a vertex. Two solid lines with arrows pointing away from the vertex are labeled  $F_{2\beta}$  (top-left) and  $\bar{F}_{1\alpha}$  (top-right). A wavy line representing a gluon, labeled  $G_{(0)\mu}^a$ , extends downwards from the vertex. To the right of the box, the expression  $= ig_s T_{\alpha\beta}^a \gamma_\mu C$  is written.

$$G\bar{u}_i u_i : C = 1, \tag{B.13}$$

$$G\bar{Q}_i Q_i : C = 1, \tag{B.14}$$

$$G\bar{U}_i \mathcal{U}_i : C = 1,$$

$$G\bar{Q}_i \mathcal{U}_i : C = 0, \tag{B.15}$$

$$G\bar{U}_i Q_i : C = 0,$$

and the same values of  $C$  for the analogous vertices with a background gluon  $\hat{G}$ .

## References

- [1] A. J. Buras, M. Spranger and A. Weiler, Nucl. Phys. B **660** (2003) 225 [arXiv:hep-ph/0212143].
- [2] T. Appelquist, H.-C. Cheng and B. A. Dobrescu, Phys. Rev. **D64** (2001) 035002, [arXiv:hep-ph/0012100].
- [3] K. Agashe, N. G. Deshpande and G. H. Wu, Phys. Lett. B **514** (2001) 309, [arXiv:hep-ph/0105084].
- [4] T. Appelquist and H. U. Yee, Phys. Rev. D **67** (2003) 055002 [arXiv:hep-ph/0211023]. [5]
- [5] P. Bucci and B. Grzadkowski, arXiv:hep-ph/0304121.
- [6] K. Agashe, N. G. Deshpande and G. H. Wu, Phys. Lett. B **511** (2001) 85, [arXiv:hep-ph/0103235]; T. Appelquist and B. A. Dobrescu, Phys. Lett. B **516** (2001) 85, [arXiv:hep-ph/0106140].
- [7] J. F. Oliver, J. Papavassiliou and A. Santamaria, Phys. Rev. D **67** (2003) 056002 [arXiv:hep-ph/0212391].
- [8] C. Macesanu, C.D. McMullen and S. Nandi, Phys. Rev. D **66** (2002) 015009 [arXiv:hep-ph/0201300].
- [9] H. C. Cheng, K. T. Matchev and M. Schmaltz, Phys. Rev. D **66** (2002) 056006 [arXiv:hep-ph/0205314].
- [10] T. G. Rizzo, Phys. Rev. D **64** (2001) 095010 [arXiv:hep-ph/0106336].
- [11] F. J. Petriello, JHEP **0205** (2002) 003 [arXiv:hep-ph/0204067].
- [12] K. Cheung, arXiv:hep-ph/0305003.
- [13] G. Servant and T. M. Tait, [arXiv:hep-ph/0206071].
- [14] H. C. Cheng, J. L. Feng and K. T. Matchev, [arXiv:hep-ph/0207125]; D. Hooper and G. D. Kribs, [arXiv:hep-ph/0208261]; G. Servant and T. M. Tait, [arXiv:hep-ph/0209262]; G. Bertone, G. Servant and G. Sigl, arXiv:hep-ph/0211342; D. Majumdar, [arXiv:hep-ph/0209277].
- [15] S.L. Glashow, J. Iliopoulos and L. Maiani Phys. Rev. **D 2** (1970) 1285.

- [16] J. Papavassiliou and A. Santamaria, Phys. Rev. **D 63** (2001) 016002. J.F. Oliver, J. Papavassiliou and A. Santamaria, hep-ph/0209021.
- [17] A.J. Buras, P. Gambino, M. Gorbahn, S. Jäger and L. Silvestrini, Phys. Lett. **B500** (2001) 161.
- [18] T. Inami and C.S. Lim, Progr. Theor. Phys. **65** (1981) 297.
- [19] A.J. Buras, W. Slominski and H. Steger, Nucl. Phys. **B238** (1984) 529, Nucl. Phys. **B245** (1984) 369.
- [20] G. Buchalla, A.J. Buras and M.K. Harlander, Nucl. Phys. **B 349** (1991) 1.
- [21] A. Muck, A. Pilaftsis and R. Ruckl, Phys. Rev. D **65** (2002) 085037 [arXiv:hep-ph/0110391].
- [22] G. Buchalla and A.J. Buras, Nucl. Phys. **B 398** (1993) 285.
- [23] A. Denner, Fortsch. Phys. **41** (1993) 307.
- [24] C. Bobeth, M. Misiak and J. Urban, Nucl. Phys. B **574** (2000) 291 [arXiv:hep-ph/9910220].
- [25] L. F. Abbott, Nucl. Phys. B **185** (1981) 189; L. F. Abbott, Acta Phys. Polon. B **13** (1982) 33; L. F. Abbott, M. T. Grisaru and R. K. Schaefer, Nucl. Phys. B **229** (1983) 372.
- [26] D. Chakraverty, K. Huitu and A. Kundu, Phys. Lett. B **558** (2003) 173 [arXiv:hep-ph/0212047].
- [27] M. Battaglia *et al.*, arXiv:hep-ph/0304132.
- [28] P. Gambino and M. Misiak, Nucl. Phys. B **611** (2001) 338 [arXiv:hep-ph/0104034].
- [29] A. J. Buras, A. Czarnecki, M. Misiak and J. Urban, Nucl. Phys. B **631** (2002) 219 [arXiv:hep-ph/0203135]. A. J. Buras, A. Czarnecki, M. Misiak and J. Urban, Nucl. Phys. B **611** (2001) 488 [arXiv:hep-ph/0105160].
- [30] A. J. Buras and M. Misiak, Acta Phys. Polon. B **33** (2002) 2597 [arXiv:hep-ph/0207131].
- [31] A. Ali and M. Misiak in [27].
- [32] T. Hurth, arXiv:hep-ph/0212304.
- [33] A.J. Buras, hep-ph/9806471, in *Probing the Standard Model of Particle Interactions*, eds. R. Gupta, A. Morel, E. de Rafael and F. David (Elsevier Science B.V., Amsterdam, 1998), page 281.

- [34] K. G. Chetyrkin, M. Misiak and M. Munz, *Phys. Lett. B* **400** (1997) 206 [Erratum-ibid. *B* **425** (1998) 414] [arXiv:hep-ph/9612313].
- [35] A. J. Buras, M. Misiak, M. Münz and S. Pokorski, *Nucl. Phys.* **B424** (1994) 374.
- [36] S. Bertolini, F. Borzumati and A. Masiero, *Phys. Rev. Lett.* **59** (1987) 180.
- [37] N. G. Deshpande, P. Lo, J. Trampetic, G. Eilam and P. Singer *Phys. Rev. Lett.* **59** (1987) 183.
- [38] A. Ali, and C. Greub, *Z.Phys.* **C60** (1993) 433.
- [39] P. Gambino and U. Haisch, *JHEP* **0009** (2000) 001 [arXiv:hep-ph/0007259]. P. Gambino and U. Haisch, *JHEP* **0110** (2001) 020 [arXiv:hep-ph/0109058].
- [40] C. Greub, T. Hurth and D. Wyler, *Phys. Rev. D* **54** (1996) 3350 [arXiv:hep-ph/9603404]. C. Greub and P. Liniger, *Phys. Rev. D* **63** (2001) 054025 [arXiv:hep-ph/0009144].
- [41] C. Greub and P. Liniger, *Phys. Lett. B* **494** (2000) 237 [arXiv:hep-ph/0008071]; C. Greub and P. Liniger, *Phys. Lett. B* **494** (2000) 237 [arXiv:hep-ph/0008071].
- [42] A. Lenz, U. Nierste and G. Ostermaier, *Phys. Rev. D* **56** (1997) 7228 [arXiv:hep-ph/9706501].
- [43] J. Kaneko *et al.* [Belle Collaboration], *Phys. Rev. Lett.* **90** (2003) 021801 [arXiv:hep-ex/0208029].
- [44] A. Ali, E. Lunghi, C. Greub and G. Hiller, *Phys. Rev. D* **66** (2002) 034002 [arXiv:hep-ph/0112300].
- [45] G. Buchalla, A.J. Buras and M. Lautenbacher, *Rev. Mod. Phys* **68** (1996) 1125.
- [46] H. H. Asatrian, H. M. Asatrian, C. Greub and M. Walker, *Phys. Lett. B* **507** (2001) 162 [arXiv:hep-ph/0103087]; H. H. Asatryan, H. M. Asatrian, C. Greub and M. Walker, *Phys. Rev. D* **65** (2002) 074004 [arXiv:hep-ph/0109140]; H. H. Asatryan, H. M. Asatrian, C. Greub and M. Walker, *Phys. Rev. D* **66** (2002) 034009 [arXiv:hep-ph/0204341]; H. M. Asatrian, K. Bieri, C. Greub and A. Hovhannisyanyan, *Phys. Rev. D* **66** (2002) 094013 [arXiv:hep-ph/0209006].
- [47] A. Ghinculov, T. Hurth, G. Isidori and Y. P. Yao, *Nucl. Phys. B* **648** (2003) 254 [arXiv:hep-ph/0208088]; A. Ghinculov, T. Hurth, G. Isidori and Y. P. Yao, arXiv:hep-ph/0211197.
- [48] M. Misiak, *Nucl. Phys.* **B393** (1993) 23; Erratum, *Nucl. Phys.* **B439** (1995) 461.

- [49] A.J. Buras and M. Münz, *Phys. Rev. D* **52** (1995) 186.
- [50] N. Cabibbo and L. Maiani, *Phys. Lett.* **B79** (1978) 109.
- [51] C.S. Kim and A.D. Martin, *Phys. Lett.* **B225** (1989) 186.
- [52] A. Ali, T. Mannel and T. Morozumi, *Phys. Lett.* **B273** (1991) 505.
- [53] G. Burdman, *Phys. Rev. D* **57** (1998) 4254.
- [54] A.J. Buras and R. Fleischer, *Phys. Rev. D* **64** (2001) 115010; A.J. Buras and R. Buras, *Phys. Lett.* **501** (2001) 223; S. Bergmann and G. Perez, *Phys. Rev. D* **64** (2001) 115009, *JHEP* **0008** (2000) 034.; S. Laplace, Z. Ligeti, Y. Nir and G. Perez, *Phys. Rev. D* **65** (2002) 094040. A. J. Buras, arXiv:hep-ph/0303060.
- [55] G. Isidori, *Int. J. Mod. Phys. A* **17** (2002) 3078 [arXiv:hep-ph/0110255]. G. D’Ambrosio, arXiv:hep-ph/0305249.
- [56] A. J. Buras, M. E. Lautenbacher, M. Misiak and M. Münz, *Nucl. Phys.* **B423** (1994) 349.
- [57] A. Alavi-Harati et al. (KTeV Collaboration), hep-ex/0009030.
- [58] J.R. Batley et al. (NA48 Collaboration), *Phys. Lett.* **B544** (2002) 97.
- [59] A. Alavi-Harati et al. (KTeV Collaboration), *Phys. Rev. D* **67** (2003) 012005.
- [60] S. Bertolini, arXiv:hep-ph/0206095.
- [61] T. Hambye, S. Peris and E. de Rafael, arXiv:hep-ph/0305104.
- [62] A.J. Buras and M. Jamin, in preparation.
- [63] S. Bosch, A.J. Buras, M. Gorbahn, S. Jäger, M. Jamin, M.E. Lautenbacher and L. Silvestrini, *Nucl. Phys.* **B 565** (2000) 3.
- [64] A.J. Buras, P. Gambino, M. Gorbahn, S. Jäger and L. Silvestrini, *Nucl. Phys.* **B592** (2001) 55.
- [65] R. Gupta, private communication.
- [66] H. Wittig, arXiv:hep-lat/0210025.
- [67] E. Gamiz, M. Jamin, A. Pich, J. Prades and F. Schwab, *JHEP* **0301** (2003) 060 [arXiv:hep-ph/0212230]. M. Jamin, J. A. Oller and A. Pich, *Eur. Phys. J. C* **24** (2002) 237 [arXiv:hep-ph/0110194]. S. Chen, M. Davier, E. Gamiz, A. Hocker, A. Pich and J. Prades, *Eur. Phys.*

J. C **22** (2001) 31 [arXiv:hep-ph/0105253]. K. Maltman and J. Kambor, Phys. Rev. D **65** (2002) 074013 [arXiv:hep-ph/0108227].